End-Of-Degree Thesis

Generation of Spin Squeezing in hybrid materials

Author:

SEBASTIÁN ROCA JERAT

Supervisors:

DAVID ZUECO LÁINEZ
FERNANDO LUIS VITALLA

Department of Condensed Matter Physics
Faculty of Science
University of Zaragoza

"*Aunque no podemos adivinar el tiempo que será,*
sí que tenemos al menos el derecho de imaginar
el que queremos que sea."

Eduardo Galeano, "Derecho al delirio"

Me gustaría agradecer y dedicar este trabajo a todas las personas que ayudaron a apartar piedras del camino durante estos cuatro años y seguro de los que quedan por recorrer. Espero que mis escuetas palabras no sean consideradas como un menosprecio a la inmensa ayuda y apoyo que me han dado, pero seguro que mi torpeza con las palabras resulta peor.

Agradecer particularmente a David y Fernando su infinita paciencia durante todo el trabajo y el interés en guiarme e introducirme en el vasto mundo de la investigación.

Contents

Introduction

The development of quantum simulators, as well as quantum technologies in general, based on atomic or molecular qubits are subject to understanding and controlling coherent interactions between the atoms. These interactions can be further exploited by driving our atomic system with an electromagnetic field; light-matter coupling has been largely studied and its control deeply consolidated in the laboratories.

We may use its quantum spin to define the qubit degrees of freedom. Here, we will do so and we will study its interaction with the electromagnetic field in the same framework for both subsystems. For this, we quantize the radiation and thus the interaction is reduced to an exchange between photons and excited states in the spin ensemble. In order to keep the radiation tunable and localized in space, cavities are often used. There, both the electromagnetic modes and the material sample are confined inside it. The basic scenario in such systems consists in the excitation and deexcitation of one spin 1/2, a two level system that realizes each qubit, via annihilation and creation, respectively, of one photon. Those states are superpositions of light and matter, i.e. cavity and spin excitations. They are known as polaritons. They are one of the most basic objects of cavity Quantum Electrodynamics (QED); the theory that studies this kind of systems. Polaritons are also present in systems with more than one two-level system, where the spin excitation is shared by all atoms in the ensemble.

However, the above description deals only with cases where the total number of excitations within the system is conserved: for each excitation created (either one photon or one spin flip in the atomic ensemble) another one is consumed and vice versa. In a more general situation symmetry does not need to hold. This is the main focus of this thesis, specifically, systems where not only the number of excitations is not conserved but neither does its parity. We will be interested in processes where one single photon can create two excitations in the spin ensemble, creating a coherent interaction between one photon and two collective spin states. This kind of process was theorized recently in the one photon two atoms case [1] but has to be seen yet in a laboratory.

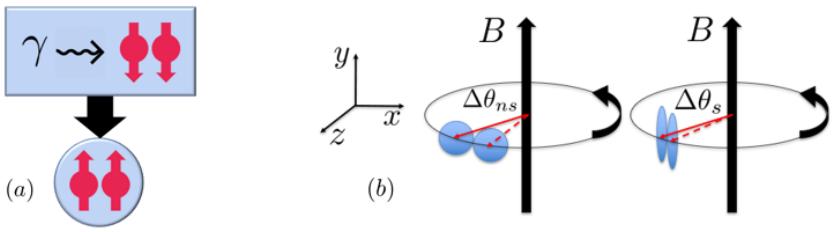

Figure 1: The coherent interaction between one photon and two spin states (a) has been shown to produce optimal spin squeezing [2]. Spin squeezed states can be represented as we do in (b): by diminishing the uncertainty in the x-direction of the spin momentum, paying the cost by the Heisenberg principle of increasing the uncertainty in the y-direction, we are able to increase the precision in the measurement ($\Delta\theta_{ns}$ for the non-squeezed state vs $\Delta\theta_s$ in the squeezed one) of spin momentum (z-direction) precession originated by the magnetic field applied in the y-direction.

One of the most appealing applications of this interaction lies in quantum sensing [3]. It has

been shown that this process creates optimal spin squeezing [2]. To introduce the concept of spin squeezed states, let's suppose that we have one spin polarized sample along the z-direction and that we apply to it a magnetic field along the y-direction. Then, by the Larmor effect, the spin momentum of the sample will rotate in the zx-plane, as it is sketched in Fig.1. If we now want to measure the Larmor frequency, or the time that this momentum takes to rotate a certain angle, we have to deal with the intrinsic uncertainty, arising from Heisenberg's uncertainty principle, in all three spin components. This uncertainty introduces an imprecision in our measurement. Due to Heisenberg's uncertainty principle, we know that uncertainties on the three spin components are bound and that they are related in such a way that they cannot be eliminated. However, we can reduce the uncertainty in one direction at the expense of increasing it in another one. For our particular case, we could reduce the uncertainty in the x-direction in order to gain precision in our measurements giving that the resulting increase in the y-direction uncertainty does not suppose a negative consequence. Such states in which the uncertainty has been "transferred" from one component to the other two are referred to as "spin squeezed" states. As the Larmor frequency is proportional to the magnetic field, one could use these states as quantum sensors to measure very subtle magnetic field changes. For this, it is necessary to find methods able to generate and optimize spin squeezing.

Besides the theoretical exploration of the one photon-two spin excitations we are also interested in its experimental implementation. After identifying the critical parameters in our models and the necessary conditions for this interaction to occur, we would review the most suitable circuits in which we could reach this situation and check if it is feasible. We will study in detail the current technological available possibilities, measuring and computing the reachable values of these parameters and finally discussing if they are enough or if improvements are needed.

1 Theoretical background

1.1 Light-Matter interaction

For our purposes it is more than sufficient start with the Dirac equation:

$$(i\hbar\not{\partial} - mc)\psi = 0 \tag{1}$$

where $\not{\partial} \equiv \gamma^\mu \partial_\mu$, being γ^μ the gamma matrices. As important remark, the Dirac equation was the first equation that jointed special relativity and quantum mechanics, being for many people the most beautiful equation in physics. Among the several achievements of this theory, maybe the most important one was to theoretically account for the the spin term which was first introduced by Pauli phenomenologically in order to explain the experimental results obtained in the well-known Stern-Gerlach experiment. This is particularly relevant for this thesis, that is devoted to the coupling of spins and light. In the non-relativistic limit, $v << c$, the Dirac equation reduces to the Pauli equation for an electron with mass m_e:

$$\mathcal{H}_{\text{Pauli}} = \frac{1}{2m_e}(\mathbf{p} + e\mathbf{A})^2 - e\phi - \frac{e\hbar}{2m_e}\boldsymbol{\sigma}\cdot\mathbf{B} \tag{2}$$

where $\boldsymbol{\sigma}$ are the Pauli matrices[1], ϕ is the Coulomb electrostatic potential, $\mathbf{A}$ is the potential vector and $\mathbf{B} = \boldsymbol{\nabla} \times \mathbf{A}$ is the magnetic field.

Hamiltonian (2) is the microscopic foundation of this thesis. It covers the interaction between light and matter in the limit stated. Our next step is to quantize the light[2]. With this aim we introduce the gauge transformations:

$$A'_\mu = A_\mu - \frac{1}{e}\partial_\mu \chi \tag{3}$$

where we have written the potential vector in its covariant notation, $A_\mu \equiv (\phi, \mathbf{A})$, as well as the partial differential, $\partial_\mu \equiv (\frac{1}{c}\partial_t, \nabla)$ and χ is some arbitrary scalar function. Equations (1) and (2) are said to be gauge invariant because they are invariant to transformations of this kind; i.e. the phase space is enlarged due to this degeneracy in the gauge choice. Fixing the gauge consists in choose certain restrictions to A_μ. For our purpose, that is, to quantize the electromagnetic field, is convenient to choose the Coulomb gauge, which imposes $\boldsymbol{\nabla}\cdot\mathbf{A} = 0$ (transversality condition). Now the field only has transversal component and satisfies $\partial_\mu\partial^\mu\mathbf{A} = 0$ and we can express the potential vector as a Fourier series:

$$\mathbf{A}(\mathbf{r}, t) = \sum_k c_k(t)\mathbf{u}_k(\mathbf{r}) \tag{4}$$

where $c_k(t)$ are the time dependent coeficients and $\mathbf{u}_k(\mathbf{r})$ orthogonal functions for the propagation mode with wave vector $\mathbf{k}$ and angular frequency $\omega_k = |\mathbf{k}|c$. If we introduce this expression in the classic electromagnetic Hamiltonian

$$\mathcal{H}_{rad} = \frac{1}{2}\int(\epsilon_0|\mathbf{E}|^2 + \mu_0|\mathbf{B}|^2)dV \tag{5}$$

[1] These matrices are $\sigma_x = \begin{pmatrix} 0 & 1 \\ 1 & 0 \end{pmatrix}; \sigma_y = \begin{pmatrix} 0 & -i \\ i & 0 \end{pmatrix}; \sigma_z = \begin{pmatrix} 1 & 0 \\ 0 & -1 \end{pmatrix}$

[2] The formal quantization of the electromagnetic field is too vast to be presented here in detail, so we restrict ourselves to this modest summary. The complete procedure can be seen in [4, 5]

and take into account the Maxwell equations $\mathbf{E} = \partial_t \mathbf{A}$ and $\mathbf{B} = \boldsymbol{\nabla} \times \mathbf{A}$, we end with the Hamiltonian for a collection of coupled harmonic oscillators:

$$\mathcal{H}_{rad} = \sum_k \frac{1}{2}(P_k^2 + \omega_k^2 Q_k^2) \tag{6}$$

where the canonical variables $Q_k \equiv (c_k + c_k^*)$ and $P_k \equiv -i\omega_k(c_k - c_k^*)$ have been introduced.

The final step is to make the change from field vectors to operators. The states that will be representate the radiation will be denoted as $|n_0, n_1, \ldots, n_k, \ldots\rangle$ where n_i stands for the number of excitations (photons) the electromagnetic mode i has with energy $\hbar\omega_i$. In doing so, we also introduce the annihilation, a, and creation, $a^\dagger$ operators:

$$a_k = \frac{1}{\sqrt{2\hbar\omega_k}}(\omega_k Q_k + iP_k); \qquad a_k^\dagger = \frac{1}{\sqrt{2\hbar\omega_k}}(\omega_k Q_k - iP_k) \tag{7}$$

which obeys the commutation relation $[a, a^\dagger] = \mathcal{I}$ and their action over the radiation states reads $a_k |n_k\rangle = \sqrt{n_k}\,|n_k - 1\rangle$ and $a_k^\dagger |n_k\rangle = \sqrt{n_k + 1}\,|n_k + 1\rangle$. As their names indicate, the operator a_k destroys one excitation in the mode k whereas $a_k^\dagger$ creates it. The quantized electromagnetic field Hamiltonian finally reads:

$$\mathcal{H}_{rad} = \sum_k (a_k^\dagger a_k + 1/2)\hbar\omega_k \tag{8}$$

The operator $a_k^\dagger a_k$ just accounts for the number of photons which exist in the mode k: $a_k^\dagger a_k |n_k\rangle = n_k |n_k\rangle$. Note that the energy in the vacuum state is non-zero; indeed $\langle 0| \mathcal{H}_{rad} |0\rangle = \sum_k \frac{1}{2}\hbar\omega_k$.

Furthermore, the expression for the quantized magnetic field is [see last term in Eq.(2)]:

$$\mathbf{B} = \sum_k \mathbf{B}_{rms}(a_k + a_k^\dagger) \tag{9}$$

being $\mathbf{B}_{rms}$ the root-mean-square magnetic field fluctuations. Thus, from this point on, for simplicity's sake, we are going to work with atoms with two relevant energetic states. These systems are refered as two-level systems (TLS) or qubits and are isomorphic to a 1/2 spin particle. If the energy difference between the two states is labelled as $\hbar\Delta$, the Hamiltonian reads:

$$\mathcal{H} = \frac{\hbar\Delta}{2}\sigma_z + \sum_k a_k^\dagger a_k \hbar\omega_k - \mathcal{H}_{int} \tag{10}$$

In fact, we will focus to magnetic molecules where the electrons are symmetrically distributed, so the electric dipole is zero and therefore we will only have the Zeeman coupling term in the interaction, which is the last term in Eq.(2).

1.2 Coupling term

Now we are going to consider that the magnetic molecules are inside a cavity, which prevents the electromagnetic modes to dissipate, with some material sample placed inside. The modes allowed can be restricted by the geometry of the cavities. Here we are going to consider only one resonant mode (single mode approximation), ω_c, so the sum in Eq.(10) can be omitted. The theory that studies the interaction between light and matter inside such a cavity is known as *Cavity QED*. The interaction intensity between the sample and the radiation is usually denoted through the parameter g, giving an interaction energy proportional to $\hbar g$. We can deduce an

expression for this parameter, following the previous discussion, supposing that the interaction occurs via Zeeman coupling:

$$\mathcal{H}_{int} = \frac{g_e \mu_B}{\hbar} \mathbf{S} \cdot \mathbf{B} \tag{11}$$

being $g_e \approx 2$ the electron g-factor, $\mu_B \equiv \frac{e\hbar}{2m_e}$ the Bohr magneton and $\mathbf{S} = \frac{\hbar}{2}\boldsymbol{\sigma}$ is the spin operator. Projecting this $\mathcal{H}_{int}$ onto the TLS basis and introducing the magnetic field $\mathbf{B}$ just quantized (Eq.(9)):

$$\mathcal{H}_{int} = \hbar g \sigma_x (a + a^\dagger) \tag{12}$$

Where, denoting as $|0\rangle$ and $|1\rangle$ the ground and excited states from our TLS, respectively, the interaction parameter has been expressed as:

$$g \equiv g_e \mu_B |\langle 0| \mathbf{S} \cdot \mathbf{B}_{rms} |1\rangle| \tag{13}$$

It indicates how likely is the spin to be led by the light from its initial state to the final one and it is clear that stronger the magnetic field, the stronger the coupling is. Eq.(12) is easy to understand: while the σ_x operator switches the spin state $|0\rangle \longleftrightarrow |1\rangle$, $(a + a^\dagger)$ does similarly for light states $|n-1\rangle \longleftrightarrow |n\rangle \longleftrightarrow |n+1\rangle$. In fact, we can express σ_x as $\sigma_x = (\sigma_+ + \sigma_-)$, being $\sigma_\pm$ the raising/lowering operators in the spin space.

1.3 Dicke model and symmetries

The most basic model in cavity QED is the *Rabi model* [6] in which we have only one TLS inside the cavity. The Hamiltoninan describing such a system is [cf. Eqs. (10) and (12)][3]:

$$\mathcal{H}_{\text{Rabi}} = \frac{\Delta}{2}\sigma_z + \omega_c a^\dagger a + g\sigma_x(a + a^\dagger) \tag{14}$$

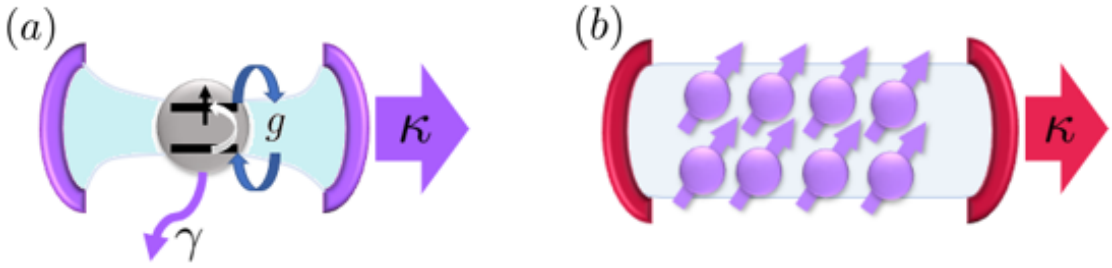

Figure 2: Schematic representation of cavity QED models: Rabi (a) and Dicke (b). The difference is the number of TLS considered inside the cavity. Moreover, in the figure of the left we represent the typical parameters present in this theory. The coupling intensity between light and matter is parametrized by g; the dissipation losses of the cavity by κ and the atomic decoherence ratio by γ.

We sketch in figure 2 the typical parameters involved in cavity QED. Generally, our system is an open system; i.e. it interacts with its environment which yields dissipation. The cavity has some dissipation ratio κ accounting for photon leakage whereas the spin sample presents an intrinsic decoherence ratio γ [7] due to the fact that the atom can deexcitate in a non radiative process, without emitting any photon to the cavity, e.g. coupling to phonons. This will be

[3] We are going to use from now on natural units where $\hbar = 1$

explored in more detail in the next section. Coming back to the Rabi model, defining the number of excitations of the system as the operator $N \equiv \sigma_+\sigma_- + a^\dagger a$, we can see that $[\mathcal{H}_{\text{Rabi}}, N] \neq 0$. The total number of excitations is not conserved in this system due to the $\sigma_+ a^\dagger$ and $\sigma_- a$ terms in Eq.(14), which creates and annihilates, respectively, excitations by pairs. However, we can change to the interaction picture [8] writing $\mathcal{H}_0 \equiv \mathcal{H}_{rad} + \mathcal{H}_{spin}$ and $\mathcal{H} = \mathcal{H}_0 + \mathcal{H}_{int}$ so, in the so-called *co-rotating frame*, the interaction term can be expressed in this picture as $\mathcal{H}^I_{int} = e^{i\mathcal{H}_0 t}\mathcal{H}_{int}e^{-i\mathcal{H}_0 t}$. If we denote as ω_q the resonant frequency for the energy difference between levels in the TLS we end with the following:

$$\mathcal{H}^I_{int} = g\left(\sigma^- a e^{-i(\omega_q+\omega_c)t} + \sigma^- a^\dagger e^{i(\omega_c-\omega_q)t} + \sigma^+ a e^{i(\omega_q-\omega_c)t} + \sigma^+ a^\dagger e^{i(\omega_q+\omega_c)t}\right) \tag{15}$$

Those terms in which the exponent is a frequency detuning, or a difference between natural frequencies, are called *co-rotating* terms and those which are formed by the sum of frequencies are called *counter-rotating* terms. If we place ourselves in the condition of resonance, or near to it, where $\omega_c \approx \omega_q$, we can neglect the counter-rotating terms due to its oscillation is much higher than the one corresponding to the co-rotating terms. This approximation is the *Rotating Wave Approximation*, or RWA for simplicity, and if we do so, we end with the *Jaynes-Cummings model*, first proposed by E.T. Jaynes and F.W. Cummings in 1963 (J.C.) [9]. Returning back to the Schrödinger picture the JC Hamiltonian is

$$\mathcal{H}_{\text{JC}} = \frac{\Delta}{2}\sigma_z + \omega_c a^\dagger a + g(\sigma^- a^\dagger + \sigma^+ a) \tag{16}$$

and now $[\mathcal{H}_{\text{JC}}, N] = 0$, the number of excitations is indeed conserved.

The RWA approximation is not alway accurate. Either by increasing the coupling, g, or considering a large number of spins, so enhancing the collective interaction (see below) we must consider the full quantum Rabi model (14). Thus, let us discuss an important symmetry of H_{Rabi}. The Rabi model conserves the parity in the number of excitations; i.e. if our initial state has an even/odd number of excitations, the only transitions allowed through Eq.(14) will be the ones which preserve that parity. This can be seen by defining the parity operator as $P \equiv \sigma_z e^{i\pi a^\dagger a}$: $[\mathcal{H}_{\text{Rabi}}, P] = 0$. Of course, $\mathcal{H}_{\text{JC}}$ keeps this symmetry, since N is conserved the parity holds.

The models introduced so far consider one two-level system. The Dicke model [10, 11] generalizes the Rabi model considering N-TLS[4]:

$$\mathcal{H}_{\text{Dicke}} = \frac{\Delta}{2}\sum_i \sigma^i_z + \omega_c a^\dagger a + g(a + a^\dagger)\sum_i \sigma^i_x \tag{17}$$

Regarding the symmetries, the Rabi model is equivalent to Dicke and therefore parity will be preserved by the latter. This implies that transitions involving an odd change in the number of excitations are forbidden. Finally, it should be noted that the RWA applied on the Dicke model results in the *Tavis-Cummings model*, i.e. the JC model in the N-TLS scenario.

2 Symmetry broken system

2.1 Break in parity conservation

In order to break the parity symmetry it is necessary to introduce some anisotropic term in (17) which could mix the operators σ_z and σ_x. Such a term and such a system are our main object

[4]We have considered that all the two-level systems have the same energy difference, the same coupling to the electromagnetic field and that they do not interact between them.

of study in this section. Hence, from this point on we will work with the same Hamiltonian that is studied in [2] to seek the optimal spin squeezing:

$$H = \frac{\Delta}{2} J_z + \frac{\epsilon}{2} J_x + \omega_c a^\dagger a + g\left(a + a^\dagger\right) J_x \tag{18}$$

This Hamiltonian differs from the Dicke model presented in Eq.(17) in the second term, which represents the effect of a magnetic flux applied externally to the system [12]. This flux originates a qubit energy bias proportional to ϵ. Adhering to the notation introduced in the previous section, Δ still denotes the energy difference between the two levels of each qubit (when $\epsilon = 0$); ω_c is the resonant mode in the optical cavity; a and $a^\dagger$ are the photon annihilation/creation operators; g is the individual coupling of each qubit to the cavity and $J_\alpha = \sum_i \sigma_\alpha^i$, $\alpha = x, y, z$, represents the total spin momentum operators (we are assuming that the ensemble is large enough to only have the total spin coupled to the cavity). The first step will be to diagonalize the qubit term in Eq.(18), namely

$$H_q \equiv \frac{\Delta}{2} J_z + \frac{\epsilon}{2} J_x \tag{19}$$

so as to gain insights in how this energy bias term, ϵ, modifies the original eigenstates and eigenvalues of the isolated qubits. The detailed analytical calculations are presented in App.A. The new energy difference between the two states of each qubit is

$$\omega_q \equiv \sqrt{\Delta^2 + \epsilon^2} \tag{20}$$

and the new eigenstates, if we denote as $|0\rangle$ and $|1\rangle$ the original qubit fundamental and first excited states, respectively, are

$$\begin{cases} |0\rangle' \equiv \cos\dfrac{\theta}{2}|0\rangle - \sin\dfrac{\theta}{2}|1\rangle & \text{(21a)} \\ |1\rangle' \equiv \sin\dfrac{\theta}{2}|0\rangle + \cos\dfrac{\theta}{2}|1\rangle & \text{(21b)} \end{cases}$$

where the angle θ has been introduced as $\sin\theta \equiv \epsilon/\omega_q$. We already see that if $\theta = 0$ we would recover the original eigenstates. In fact, this will imply that ϵ is zero and we will go back to the Dicke model. This angle then denotes the anisotropy present due to the magnetic flux applied respect to the natural energy difference in each qubit and which mixes the two original energy levels. The spin operators now will be modified as

$$\begin{cases} \sigma_z^i \to \hat{\sigma}_z^i & \text{(22a)} \\ \sigma_x^i \to \cos\theta\hat{\sigma}_x^i + \sin\theta\hat{\sigma}_z^i & \text{(22b)} \end{cases}$$

Hence, with the qubit Hamiltonian (19) diagonalized and the spin operators transformed according to Eq.(22), the complete Hamiltonian (18) reads:

$$\hat{H} = \omega_q \hat{J}_z + \omega_c a^\dagger a + g(\cos\theta \hat{J}_x + \sin\theta \hat{J}_z)(a + a^\dagger) \tag{23}$$

The quantum states will be labelled as $|n, j, m\rangle \equiv |n\rangle \otimes |j, m\rangle$, like in [2], being $|n\rangle$ the Fock state and $|j, m\rangle$ the collective spin state, where j denotes the total angular momentum, $j = N_s/2$ (N_s is the number of qubits in the sample), and m indicates the third component eigenvalue of the total spin momentum, i.e. how many qubits are excited, ranging from $m = -j$, for all qubits in its ground state, to $m = +j$, corresponding to all the qubits excited. However, for simplicity's

sake, the number j, which will remain constant once we have fixed the ensemble size, will be omitted.

Once the Hamiltonian has been characterized according to our interest, having only one term describing the qubit space, another one for the normal mode in the cavity and one last term for the interaction between the two subsystems, we proceed to numerically compute the eigenenergies and eigenstates. As we can see in Fig.3, two gripping anticrossings are spotted. The first one (plot labeled as (c) in Fig.3), at $\omega_c = \omega_q$, corresponds to the *Rabi oscillations* [13] which entangle the states $|n = 0, m = -j + 1\rangle$ and $|n = 1, m = -j\rangle$. In this condition, the system oscillates between having one photon in the normal mode with no qubits excited and no photons with one collective excitation in the sample. As the number of excitations is conserved, we can understand this anticrossing treating the system in this region with an effective Hamiltonian like $\mathcal{H}_{\text{JC}}$ in Eq.(16). We recall that not just one single qubit is being excited by the photon but a superposition of all states that contain one qubit in its excited state and this not only occurs for one photon. We can see in the plot (a) that there are anticrossings all the way up in $\omega_c = \omega_q$, entangling more states due to the new possibilities of combination of excited states between the sample and the light but, in essence, we keep finding oscillations in the system between the creation of one photon by deexciting one qubit and vice versa.

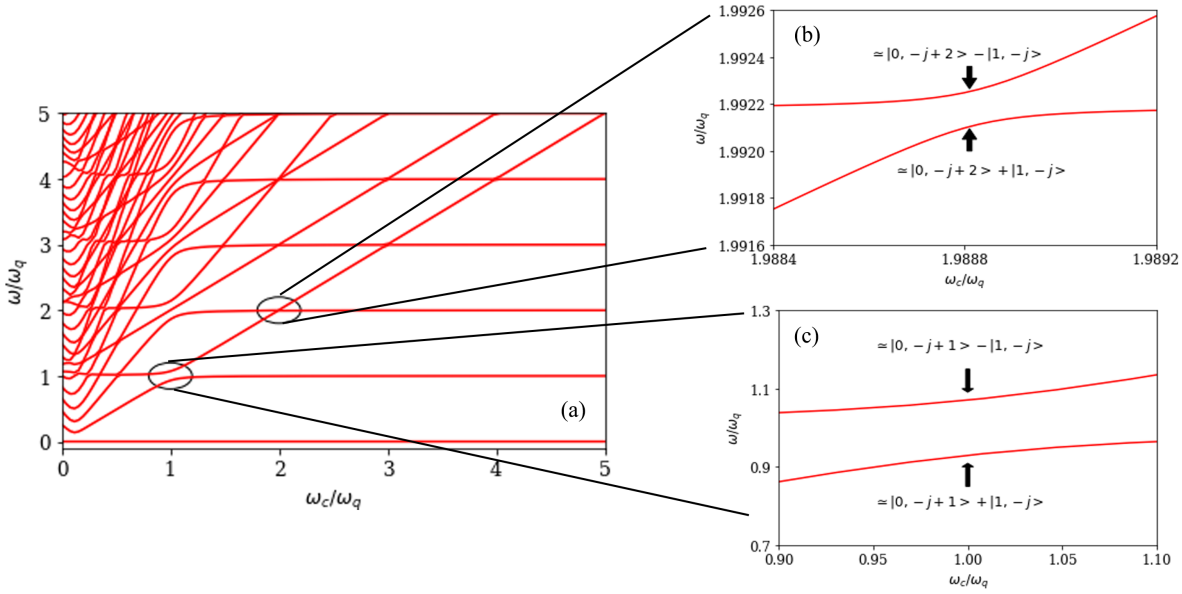

Figure 3: (a) Energy spectrum of the Hamiltonian for $N_s = 20$ spins in the sample. The parameters used were $g\sqrt{N}/\omega_q = 0.1$ and $\theta = \pi/4$. The circles indicate the anticrossings explained in the main text, namely: (b) the entanglement between the $|n = 0, m = -j + 2\rangle$ and $|n = 1, m = -j\rangle$ states which is the main object under study in this thesis and (c) the *Rabi oscillation*.

If we continue increasing the cavity normal mode frequency up to $\omega_c \approx 2\omega_q$ we find [See Fig.3(b)] that one single photon can create two excitations in the spin ensemble. Equivalently, these two excitations together will create one single photon in the cavity, originating in this scenario oscillations like the Rabi ones. Such a coherent interaction remains to be seen in the laboratory yet but the theoretical birth of this process occurred few years ago in [1] where it

was explored in the one photon and two atoms case. Recently, in [2], the authors extended this possibility to a more general situation where an arbitrary number of photons and qubits is present in the cavity. The collective interaction can be seen in Fig.3(a) through the vertical $\omega_c = 2\omega_q$ where a series of anticrossings involving entanglements between states differing by an odd number of excitations can be seen, although much narrower than the ones in $\omega_c = \omega_q$. This feature will be explored later, but already gives us a glimpse about the subtlety of the process: in order to encounter the oscillation $|n, m+2\rangle \longleftrightarrow |n+1, m\rangle$ we need to be very precise in the resonant frequency because, as can be seen in Fig.3(b), the splitting promptly broadens and the superposition of these kets is lost.

Looking closer into this resonant frequency, $\omega_c \approx 2\omega_q$, we see that the approximate symbol was not casually introduced, there is indeed a shift in this condition [See Fig.3(b)]. This effect is due to the increasing in the coupling between matter and light and is also seen in the anticrossing splitting amplitude. The results of the analysis of these two effects are presented in Fig.5. The splitting broadening, Ω, is found to increase with the coupling and the ensemble size as $\Omega \propto g^3 N$, a result that coincides with the one obtained in [2] and that shows how the collective interaction between spins in the ensemble enhances optical effects. Hence, in order to be able to see experimentally this anticrossing, one needs a sufficiently large splitting in the transmission spectrum reflecting this phenomenon.

Thus, to achieve it, increasing the coupling as much as possible should be our main interest. Although we will delve into this in the next section when we study the dynamics of the system, we can already anticipate that we have to be careful about increasing excessively this coupling because all the theory developed and reviewed until now considers a sufficiently weak interaction between light and matter. In fact, we can see also in Fig.5 that the resonant condition $\omega_c = 2\omega_q$ shifts downwards as $\omega_c/\omega_q \propto -(g\sqrt{N}/\omega_q)^2$. This could account for the need of more interaction terms in the Hamiltonian (23) as it also occurs in the *Rabi oscillations* as have been observed in numerical simulations. However, the experimental accessible coupling strengths are, as we will see later, much less than the required to slip from our theory framework.

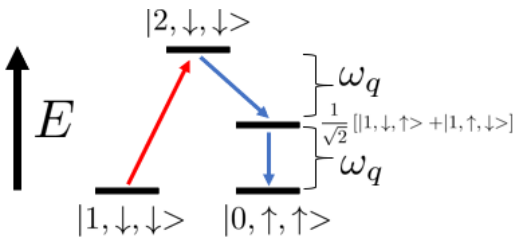

Figure 4: Transition between states $|1,\downarrow,\downarrow\rangle$ and $|0,\uparrow,\uparrow\rangle$ with its possible intermediate virtual processes.

2.2 Effective model close to the anticrossing

With the aim of better analyzing this resonance before getting into the dynamics, we turn to develope an effective Hamiltonian. If we restrict ourselves to the $\omega_c \approx 2\omega_q$ proximity, the coupling between an odd number of excitations differing states, specifically the $|n, m+2\rangle \longleftrightarrow |n+1, m\rangle$ anticrossing, will be via a third order process. As it is sketched in Fig.4, considering for simplicity a situation with only two TLS in the sample, for this system to couple the states $|1,\downarrow,\downarrow\rangle$ and $|0,\uparrow,\uparrow\rangle$, it has to go through three intermediate virtual processes. In this example, first and foremost, a photon is created breaking both the parity symmetry and the number of excitations conservation (red arrow), allowing the anticrossing to occur after the other two transitions (blue

arrows) which are more "intuitive": one of the photons is consumed exciting one spin and then the remaining photon is also consumed to excite the last spin. Actually, this is not the only possibility; in the supplementary materials of [1] there are all the possible combination of virtual processes. Thus, taking into account this order of interaction and the fact that it is created/annihilated one photon to annihilate/create excitations by pairs in the spin ensemble, we can approximate the interaction Hamiltonian as

$$\hat{H}_{\text{eff}}^{\text{int}} \approx g_{\text{eff}}(aJ^{\dagger 2} + h.c.) \tag{24}$$

where this effective coupling is found in the literature [2] to be

$$g_{\text{eff}} = -\frac{4g^3\cos^2\theta\sin\theta}{3\omega_q^2}N \propto g\left(\frac{g\sqrt{N}}{\omega_q}\right)^2 \tag{25}$$

as well as Eq.(24) itself computed via perturbation theory. The effective coupling dependence is numerically confirmed in Fig.5 and is one of the most important parameters in this discussion.

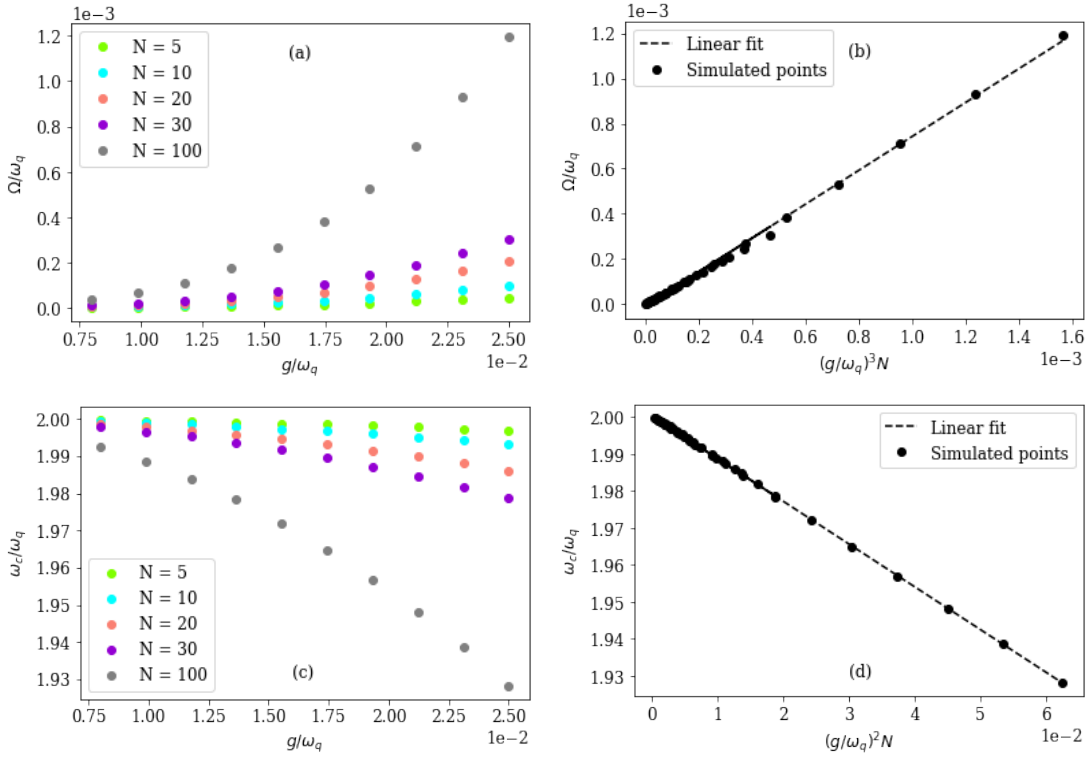

Figure 5: (a) Splitting amplitude for the $|n, m+2\rangle \longleftrightarrow |n+1, m\rangle$ anticrossing for different values of g and different sizes. (b) Direct proportionality between the splitting and g^3N. (c) Here we show how the resonant condition for the cavity frequency varies as the coupling and the ensemble size are increased. (d) Again we obtain a linear dependence, decreasing from $\omega_c = 2\omega_q$ as g^2N increases up to nearly a 10% for $g\sqrt{N}/\omega_q \approx 0.25$ which is an extremely large coupling. The points shown both in (b) and (d) are the same plotted in (a) and (c), respectively.

A further approximation consists in the so called Holstein-Primakoff transformation [14, 15] which enables to map the total momentum operators into bosonic ones. This transformation can be seen as the treatment of an ensemble of N qubits (assuming N to be sufficiently large) as a quantum oscillator. If we remain in the low polarization limit (only a small number of

TLS excited), we can consider the spin excitations as excitations in a Fock space mediated by creation and annihilation operators, denoted here as $b^\dagger$ and b, respectively. While a Fock space is an infinite-dimensional space, the spin space is finite-dimensional; that is why we need to be in the low polarization limit. If we were in a situation with a high number of TLS excited, we would be close to the "saturation of the ladder" (understanding this "ladder" as the accessible energetic levels) and the transformation would not be valid. The relation between the spin and bosonic operators can expressed as

$$J_z \sim b^\dagger b; \qquad J_+ = J_x + iJ_y \sim b^\dagger; \qquad J_- = J_x - iJ_y \sim b \tag{26}$$

and we can express Eq.(24) as

$$\hat{H}_{\text{eff}}^{\text{int}} \approx g_{\text{eff}}(ab^{\dagger 2} + h.c.) \tag{27}$$

Finally, the total Hamiltonian (23) can be approximated by:

$$\hat{H}_{\text{eff}} = \omega_q b^\dagger b + \omega_c a^\dagger a + g_{\text{eff}}(ab^{\dagger 2} + h.c) \tag{28}$$

This is the Hamiltonian which we will use next to study the system dynamics.

2.3 Transmission

A typical experimental technique for resolving the light-matter coupling is by means of transmission experiments. In this section we explain the theoretical background of them. We also show the conditions for resolving the $|n+1, j\rangle \to |n, j+2\rangle$ anticrossing. For this we introduce an external driving that consists of a plane electromagnetic wave which intensity can be related to the photon leakage of the cavity, κ, by a proportionality constant $\alpha > 1$, giving that the input is greater than the cavity losses:

$$\hat{H}_{\text{ext}} = \alpha\kappa(e^{i\omega t} + e^{-i\omega t})(a + a^\dagger) \tag{29}$$

Thus, the total Hamiltonian to be studied is now:

$$\hat{H}_{\text{T}} = \hat{H}_{\text{eff}} + \hat{H}_{\text{ext}} = \omega_c a^\dagger a + \omega_q b^\dagger b + g_{\text{eff}}(ab^{\dagger 2} + a^\dagger b^2) + \alpha\kappa(e^{i\omega t} + e^{-i\omega t})(a + a^\dagger) \tag{30}$$

The system will also be affected by spin decoherence [7], with rate γ. In order to study the dynamics, we have to take into account the interaction of our system with the environment. If losses are low enough (they are) the influence of dissipation can be cast in a Master equation like [2, 8, 16]:

$$\dot{\rho} = -i[\hat{H}_{\text{T}}, \rho] + \kappa\mathcal{D}_\rho[a] + \gamma\mathcal{D}_\rho[b] \tag{31}$$

where $\mathcal{D}_\rho[a] = \left(a\rho a^\dagger - \frac{1}{2}\{a^\dagger a, \rho\}\right)$ and $\mathcal{D}_\rho[b] = \left(b\rho b^\dagger - \frac{1}{2}\{b^\dagger b, \rho\}\right)$ are the dissipators, operators that involve the photon loss (that is why the annihilation operator a is there) in the cavity due to dissipation and the loss of excited states (same for b) in the qubit sample due to decoherence, respectively. However, the solution that we seek it is not for the density matrix, ρ, but for the mean value of some operators which will be of interest to compute the transmission factor, given by:

$$t = -i2\pi\kappa\frac{1}{\alpha\kappa}\langle a\rangle \tag{32}$$

Hence, we will be interested in calculating $\langle a \rangle$. But, as we will see and it is depicted in detail in App.B, we will also need $\langle b^2 \rangle$ and $\langle b^\dagger b \rangle$. The equation of motion for these values is, also derived in App.B:

$$\frac{d}{dt}\langle \theta \rangle = +i\left\langle [\hat{H}_T, \theta] \right\rangle + \gamma \left\langle \mathcal{D}_\theta^\dagger[b] \right\rangle + \kappa \left\langle \mathcal{D}_\theta^\dagger[a] \right\rangle \tag{33}$$

where

$$\left\langle \mathcal{D}_\theta^\dagger[A] \right\rangle = \left\langle A^\dagger \theta A \right\rangle - \frac{1}{2}\left\langle \{A^\dagger A, \theta\} \right\rangle \tag{34}$$

giving us the following closed system of equations (see App.B):

$$\begin{cases} \frac{d}{dt}\langle a \rangle = -\left(i\omega_c + \frac{\kappa}{2}\right)\langle a \rangle - ig_{\text{eff}}\langle b^2 \rangle - i\alpha\kappa\left(e^{i\omega t} + e^{-i\omega t}\right) & \text{(35a)} \\ \frac{d}{dt}\langle b^2 \rangle = -i2\omega_q \langle b^2 \rangle - i2g_{\text{eff}}\left\langle a\left(2b^\dagger b + 1\right)\right\rangle - \gamma\langle b^2 \rangle & \text{(35b)} \\ \frac{d}{dt}\left\langle b^\dagger b \right\rangle = i2g_{\text{eff}}\left(\left\langle a^\dagger b^2 \right\rangle - \left\langle a b^{\dagger 2} \right\rangle\right) - \gamma\left\langle b^\dagger b \right\rangle & \text{(35c)} \end{cases}$$

To obtain the solution of these equations we start getting rid of the oscillating terms applying the Rotating Wave Approximation (RWA):

$$\langle A \rangle = \left\langle \tilde{A} \right\rangle e^{-i\omega t} \implies \frac{d}{dt}\langle A \rangle = \frac{d}{dt}\left\langle \tilde{A} \right\rangle e^{-i\omega t} - i\omega \left\langle \tilde{A} \right\rangle e^{-i\omega t} \tag{36}$$

Besides, we use mean field decoupling to get a closed set of equations.

$$\langle AB \rangle = \langle A \rangle \langle B \rangle \tag{37}$$

After the application of these approximations (see App.B) the stationary averages of (35) are the solution of:

$$\begin{cases} \langle \tilde{a} \rangle = -\frac{i2}{\kappa}\left[\alpha\kappa + g_{\text{eff}}\left\langle \tilde{b}^2 \right\rangle + (\omega_c - \omega)\langle \tilde{a} \rangle\right] & \text{(38a)} \\ \left\langle \tilde{b}^2 \right\rangle = -\frac{i2}{\gamma}\left[g_{\text{eff}}\langle \tilde{a} \rangle\left(2\left\langle b^\dagger \tilde{b} \right\rangle + 1\right) + \frac{1}{2}(2\omega_q - \omega)\left\langle \tilde{b}^2 \right\rangle\right] & \text{(38b)} \\ \left\langle b^\dagger \tilde{b} \right\rangle = -\frac{i2}{\gamma}\left(\langle \tilde{a} \rangle \left\langle \tilde{b}^{\dagger 2} \right\rangle - h.c.\right) & \text{(38c)} \end{cases}$$

This solution is:

$$\langle a \rangle = \frac{-i\alpha\kappa}{\frac{\kappa}{2} + i(\omega_c - \omega) + \frac{2g_{\text{eff}}^2\left(2\langle b^\dagger b \rangle + 1\right)}{\gamma + i(2\omega_q - \omega)}} \tag{39}$$

$$\left\langle b^\dagger b \right\rangle = \frac{8g_{\text{eff}}^2 |\langle a \rangle|^2}{\gamma^2 + (2\omega_q - \omega)^2 - 16g_{\text{eff}}^2 |\langle a \rangle|^2} \tag{40}$$

which yields a third order equation for $\langle a \rangle$. This set has 3 solutions. Only one is physically meaningful (see App.B.4)

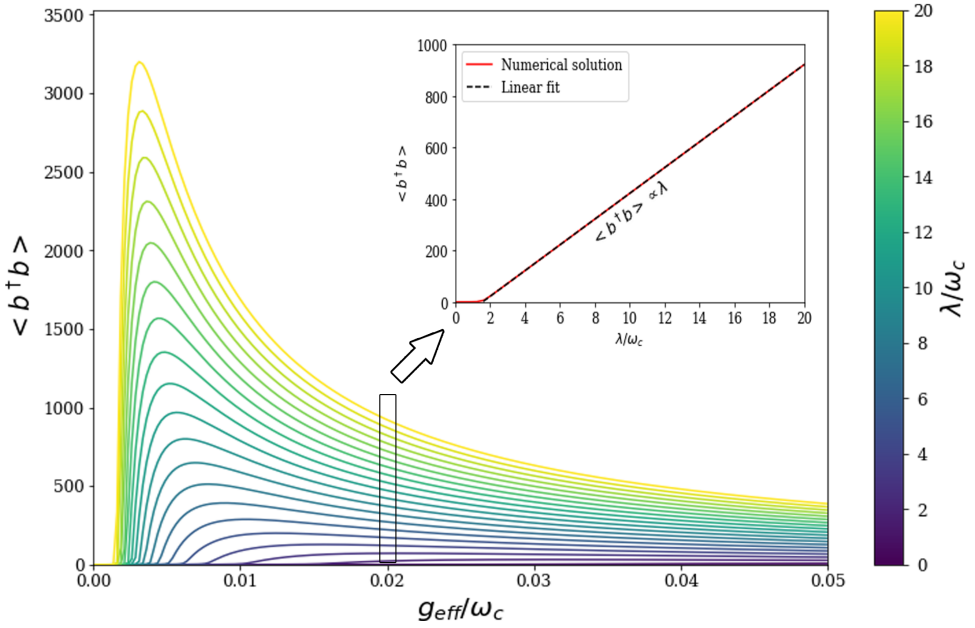

Figure 6: We show the $\langle b^\dagger b\rangle$ dependence on the effective coupling g_{eff} and the external driving intensity $\lambda = \alpha\kappa$. The inset show that $\langle b^\dagger b\rangle$ turns out to be proportional to λ. The parameters used were $\gamma/\omega_c = \kappa/\omega_c = 0.5$ in both graphs and $g_{\text{eff}}/\omega_c = 0.02$ in the inset.

In Fig.6 we plot $\langle b^\dagger b\rangle$ at resonance $\omega = \omega_c = 2\omega_q$. We observe a pronounced peak in the spin mean occupation number when $\gamma \sim 4g_{\text{eff}}|\langle a\rangle|^2$ which increases its height as we increase the driving intensity, denoted as $\lambda = \alpha\kappa$. As it is expected, the effective coupling needs to be sufficiently large to produce some interaction between the sample and the radiation yielding a finite $\langle b^\dagger b\rangle$. We also obtain that, for a sufficient large coupling g_{eff}, $\langle b^\dagger b\rangle$ is proportional to this intensity, scaling linearly with λ. This is actually an important result that will be useful in further discussions. If we put together Eq.(32) and Eq.(39) we get the following expression for the transmission:

$$t = \frac{-2\pi\kappa}{i(\omega_c - \omega) + \frac{\kappa}{2} + \frac{2g_{\text{eff}}^2(2\langle b^\dagger b\rangle + 1)}{\gamma + i(2\omega_q - \omega)}} \tag{41}$$

As we discussed in the first section, in the *Rabi oscillation* case, the coupling between the states of our interest will be represented in the transmission spectrum as two well-resolved peaks. These peaks could merge into one if the coupling is extremely small or the dissipation terms, γ and κ, too big. These two peaks will be symmetric respect to the resonant condition, here: $\omega = \omega_c = 2\omega_q$. We can check this by numerically solving Eq.(41), as we show in Figure 7.

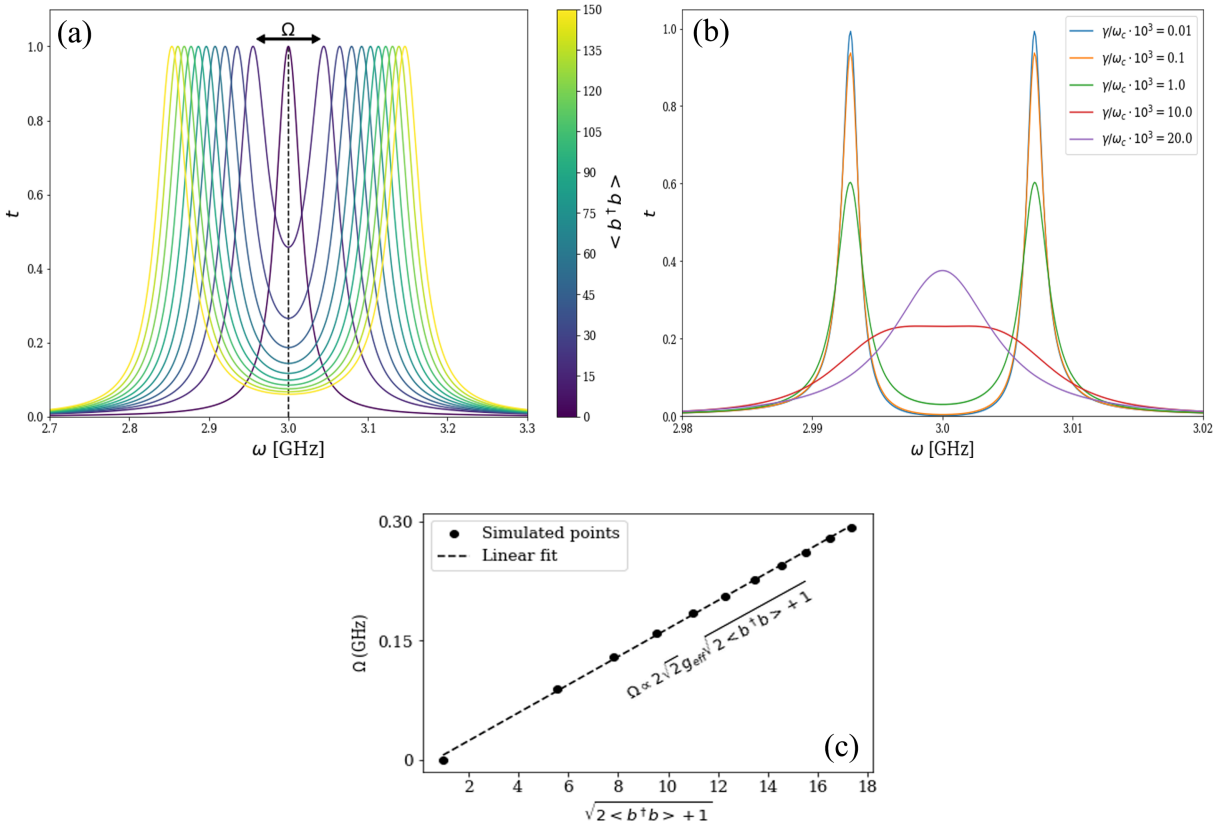

Figure 7: (a) Normalized transmission peaks obtained for $\omega_c/\omega_q = 2$, $\kappa/\omega_c = \gamma/\omega_c = 0.01$ and $g_{\text{eff}}/\omega_c = 0.002$ as we vary the driving frequency ω and the mean occupation number $\langle b^\dagger b \rangle$. Each curve has been rescaled for a better comparison between them. (b) We can see how the double peak merges into a single one as we increase the decoherence rate γ. We find that the critical value is around $\Omega \approx \frac{2}{3}\gamma$. The parameters used were $g_{\text{eff}}/\omega_c = 1/600$, $\kappa/\omega_c = 10^{-3}$ and $\langle b^\dagger b \rangle = 0$. (c) Splitting width, Ω in (a), as function of $\sqrt{2\langle b^\dagger b \rangle + 1}$.

In Fig.7 (a), we see that initially, for null mean occupation number, $\langle b^\dagger b \rangle = 0$, we only obtain one transmission peak. This would tell us that the coupling is too weak to induce by itself the transition $|n, m+2\rangle \longleftrightarrow |n+1, m\rangle$. However, as we increase $\langle b^\dagger b \rangle$, for example increasing the driving intensity as we saw in Fig.6, we obtain a progressive splitting of the two peaks, Ω. This parameter appears subtly in Eq.(41) as

$$\left(\frac{\Omega}{2}\right)^2 \propto 2g_{\text{eff}}^2 \left(2\left\langle b^\dagger b \right\rangle + 1\right) \tag{42}$$

This relation is confirmed numerically in Fig.7 (c). Besides, the decoherence rate γ also sets if we obtain two well differentiated peaks or only one as it can be seen in Fig.7 (b). We find that increasing γ modifies the transmission spectrum until we reach $\gamma \approx \frac{3}{2}\Omega$ when the double peak merges into a single one. The challenge now consists in attaining a Ω large enough through the effective coupling as well as the largest $\langle b^\dagger b \rangle$ possible, although both are bounded [cf. Eq.(39) & Eq.(40)], to surpass the previous condition. Furthermore we have to consider that we also need the largest possible splitting because of the finite sensitivity of actual devices.

3 Experimental setup

The theory described in the previous two sections allows estimating the coupling between sample and cavity that one needs to attain in to observe the anti-crossing associated with the creation of 2 excitations in the spin ensemble by a single photon. This condition comes from Eq.(25), where the collective coupling, $g\sqrt{N}$, needs to be comparable to the qubits' transition frequency to make this phenomenon observable. This effective term is what determines the peak splitting in the transmission spectrum (See Eq.(41) and Eq.(42)), which characterizes the coherent coupling between the two states we seek. We can already see that this constitutes a very demanding condition: in addition of reaching a collective coupling comparable to ω_q, one also needs a strong single spin coupling to the cavity. Keeping this in mind we should aim for the optimal architecture of the cavity to achieve the highest possible coupling. The experimental platform that was considered throughout Sec.2 is a coplanar waveguide resonator (CPW). This device has been shown to be really efficient in this endeavour as well as being a feasible architecture for quantum computation[17–20]. In this section we will explore in detail the CPW as well possible improvements that can be brought about by introducing constrictions; we will explore the reachable parameters with the current accessible technology to later discuss if the anti-crossing could be detected and finally we will discuss what further feasible improvements could be done.

3.1 Coplanar waveguide resonators (CPW) and nanoconstrictions

As we introduced in Sec.1, an electromagnetic resonator consists in an optical cavity, in our case a section of coplanar waveguide coupled to external feed lines (input and output) through capacitors. These capacitors act as "mirrors" that trap only the radiation modes whose wavelenghts match the dimensions of the resonator, being the cavity's geometry what fixes the resonant frequencies allowed. The photons inside these cavities range in the region of 1-10 GHz with long life times [19]. The central line consists of a niobium superconducting line, refrigerated below the critical temperature, 9 K, which allows to suppress losses due to resistivity increasing the quality factor. This factor, Q, accounts for the ratio between the resonant frequency and the dissipation losses. In addition, this line is surrounded by two Nb planes that prevent the central line to be perturbed by external electromagnetic noise. All these conductor components are on top of a dielectric substrate, usually sapphire (Al_2O_3).

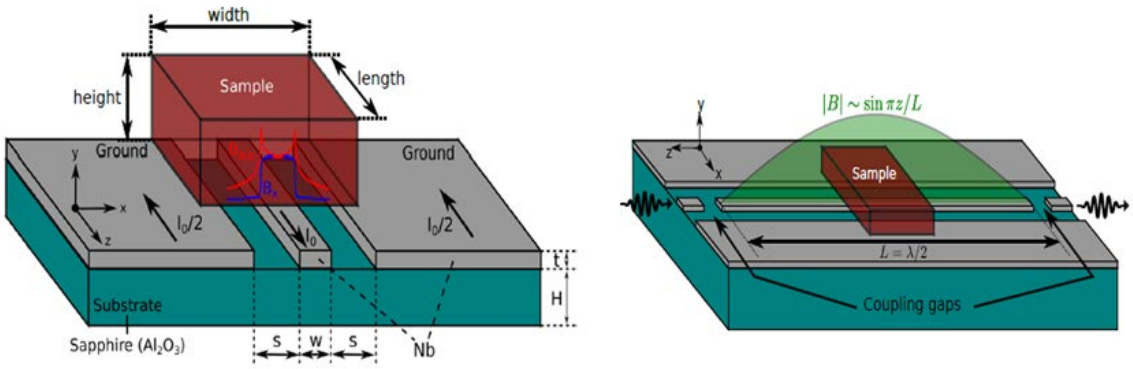

Figure 8: Graphical representation of a coplanar waveguide resonator (CPW). In the left figure we present the front view where the geometrical parameters both from the resonator and the sample are depicted as well as the direction of the electrical current. In the right one we show a side view with the first harmonic mode of the magnetic field. Reprinted from [20].

As it is shown in Fig.8, the current through the central line will create a magnetic field around it that will interact with the sample. This magnetic field will be maximum at the center of the line and larger the closer is the sample to the line in the vertical direction. The coupling of the sample to the resonator is intrinsically dependant of this field intensity through the Zeeman effect as it was shown in Sec.1. The couplings reported in the literature [19, 20] for single spins $1/2$ with this set-up are found to be around $1 - 10\ Hz$ for central line widths of $15\ \mu m$. Since typical photon resonance frequencies are of the order of a few GHz, this results to be too weak for our proposal. One way of enhancing the magnetic field and so, the single spin coupling, consists in narrowing as much as possible the central line. By confining in this way the supercurrent, the energy density and therefore the interaction between the spins and the cavity is enhanced. One way of effectively achieve this consists in the introduction of constrictions in the central line, narrowing them down to 10 nm and thereby improving the single spin coupling up to two orders of magnitude [18, 20]. In Fig.9 we show the physical implementation of one nanoconstriction in a CPW via nanolitography. Galium ions, Ga^+, are used to locally mill down the transmission line, with resolutions of a few nm. In order to avoid unwanted electrical discharges due to the presence of ions, a Platinum bridge is built between the line and the ground wire during the deposition. This process is divided in two phases: first, the regions labeled as 2-3 and 1-4 in Fig.9.C are made with less resolution but faster and then, the most important region, labeled as 1-2, employs the most of the time for accuracy's sake. Once the constriction has been made, the Pt bridge is removed. The dimensions of the constriction that was used to measure the data we will analyze next are shown in the image D of the same figure. Note that we go from the original 15 μm central line down to about 150 nm, 100 times narrower, being this possibly further exploited as we will explore later. About the resonator's original parameters, namely the resonant frequencies and the quality factor, it is shown that the introduction of the constriction does not suppose a significant perturbation [18, 20] so the benefits outweigh the drawbacks.

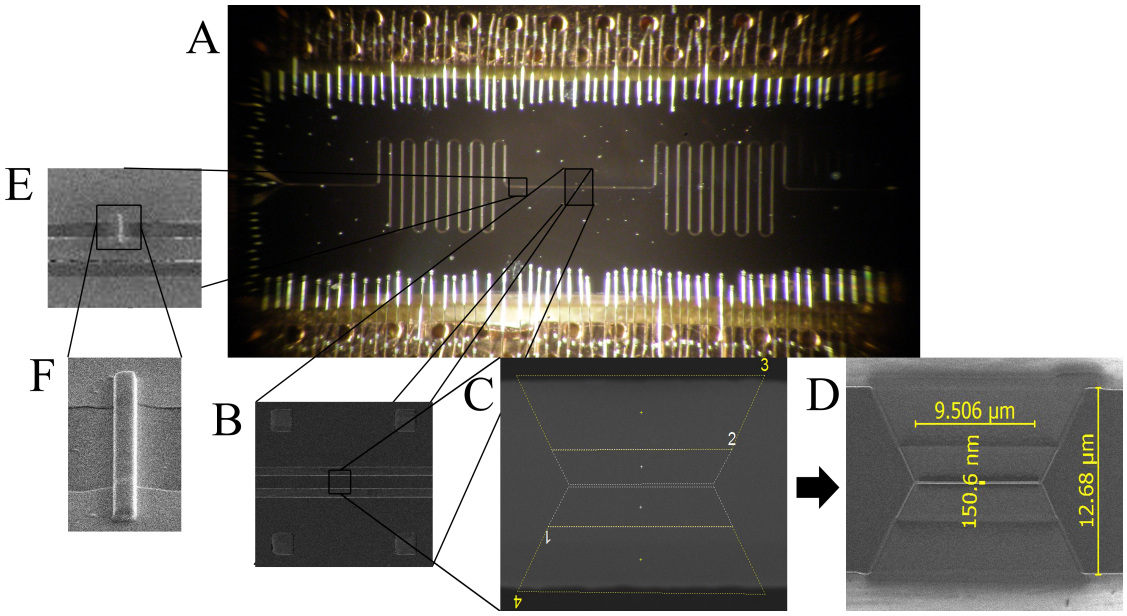

Figure 9: Circuit used to obtain the data analyzed. (A): general overview of the resonator where the curves in the superconducting line gives the total length desired to obtain the precise resonant frequencies we want. The capacitor gaps are at each extreme of the line. (B), (C), (D): central point of the line where the constriction is made in order to profit the maximum intensity magnetic field. (E), (F): the platinum bridge that avoids discharges during the fabrication of the circuit and is removed afterwards.

3.2 Measurements and data analysis

Now that the device which was used to obtain the data has been presented, we proceed to present the measurements performed and its pertinent analysis. The microwave transmission through the device was measured using a network analyzer (Fig.10), which ports 1 and 2 were conected to the feed lines of the superconducting resonator. One port for the signal input (an electromagnetic wave ranging from 0.1 GHz to 3 GHz) and the other port to detect the transmission through the cavity.

Figure 10: Network analyzer employed to measure the transmission.

About the sample deposited on the resonator, we worked in this case with organic free rad-

ical molecules which act as two level systems (or a 1/2 spin) from 2,2-diphenyl-1-picrylhydrazyl, known as DPPH. The procecure to deposit the sample in the nanoconstriction is really accurate and the technique employed was dip-pen nanolithography. In Fig.11 we show the best result of various deposition tries to obtain the maxixum number of molecules near the constriction. Being this zone so small in comparison with the drop it is not trivial to place it. Moreover, the electrostatic interactions between the circuit and the sample make the latter assemble not always in the same place. In our case the number of spins deposited was $N = 3.1 \times 10^9$. The circuit transmission resonances were measured for different magnetic fields, which bring the spins to resonance with the cavity. Lorentzian fits of these resonances provide the quality factor, $Q = f_0/\kappa$, and the resonance frequency f_0 as a function of magnetic field. From this we can obtain the cavity dissipation κ as a function of magnetic field. This is what is shown in Fig.12 where the Lorentzian fit used was Eq.(43) [20] and the frequency that appears in the x axis is the magnetic field frequency, $\Omega/2\pi = -g\mu_B B_z/h$, where the giromagnetic ratio $g = 2.02745$, μ_B is the Bohr magneton, B_z the magnetic field and h the Planck constant.

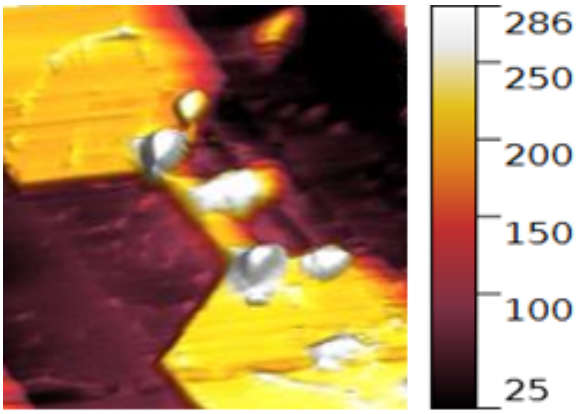

Figure 11: Sample deposition by dip-pen nanolithography.

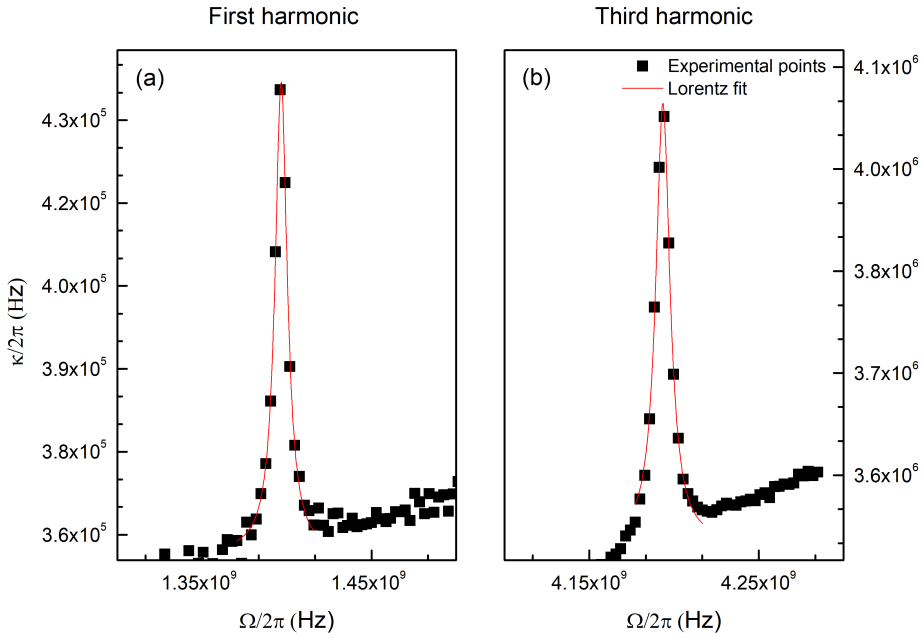

Figure 12: Fits using Eq.(43) of the data measured for the first harmonic (a) and the third (b). It can be seen how the higher magnetic field in the third harmonic produces a higher dissipation in the cavity, about one order of magnitude more.

$$\kappa \approx \kappa_0 + \frac{G^2\gamma}{(\omega_n - \Omega)^2 + \gamma^2} \tag{43}$$

We present the data collected for the first and third modes of the resonator. As we explained before, the geometry of the cavity only allows certain electromagnetic modes to propagate. However, the spacial distribution of each mode is different and therefore also will be its interaction with the sample. In Fig.13 we can see why these modes were considered and not the second harmonic which presents a magnetic field node where the sample is placed, near the constriction. Having a node in this zone implies no field intensity and so no interaction with the sample and no coupling. The first and third harmonics, on the contrary, present a maximum in its intensity there.

Parameters	Resonant mode 1	Resonant mode 3
$\omega_q/2\pi$	1.397 GHz	4.193 GHz
$\kappa/2\pi$	0.434 MHz	4.021 MHz
$\gamma/2\pi$	4.372 MHz	5.071 MHz
$g/2\pi$	116.28 Hz	191.12 Hz

Table 1: Parameters fitted from experimental data. The single spin coupling is stronger in the third harmonic as it is also greater the resonant frequency. The T_2^{-1} decoherence time, γ, remains similar due to the only change between modes corresponds to the cavity parameters, not to the sample's. We can see this in the cavity's dissipation term, κ, which indeed is increased with the mode.

The parameters obtained from the fits correspond to the decoherence rate T_2^{-1} of the sample, γ, the collective coupling of all the spins to the cavity, G, and the resonant frequency which in this case is the same for the cavity, ω_c, and the qubit, ω_q. Recall that we are interested in the resonance condition $\omega_c = 2\omega_q$ but here we are obtaining the achievable magnitudes for the single spin coupling in order to estimate if with this technology we could perform an experiment to observe that phenomenon. In the Table 1 we show the values obtained for these parameters. The value of single spin coupling, g, was computed from the collective coupling through $G = g\sqrt{N_{eff}}$, where N_{eff} accounts for the effective ensemble size due to thermal polarization. As we are at non-zero temperature, there will be spins that are in their excited state by thermal excitation and they will neither contribute to the transmission nor to the coupling measured. The experiment was realized at $T = 4.2\ K$ so the effective ensemble size:

$$N_{eff} = \left|\frac{S_z(T)}{S}\right| N \tag{44}$$

$$\frac{S_z(T)}{S} = \frac{e^{-\beta\epsilon_0}}{Z}(-1) + \frac{e^{-\beta\epsilon_1}}{Z}(+1) = \frac{e^{-\beta\epsilon_1} - e^{-\beta\epsilon_0}}{e^{-\beta\epsilon_1} + e^{-\beta\epsilon_0}} = \frac{e^{-\beta\omega_q} - 1}{e^{-\beta\omega_q} + 1} \tag{45}$$

It is evident that the lower the temperature, the closer to unity the quotient in Eq.(45) becomes; i.e., in the limit $T \to 0$ all the spins in the ensemble will be in their ground state and therefore all of them could absorb photons from the cavity.

Hence, we can now obtain the fundamental parameter that will give us the information about if we could be able to observe the interaction we seek. This parameter was introduced in section 2 as the effective coupling, g_{eff}, in the resonance condition, $\omega_c = 2\omega_q$, and which is

related with the single spin coupling through Eq.(25). Taking into account that in our sample (See Fig.11) there were $N = 3.1 \times 10^9$ spins, we present in Table 2 the values for the effective size and coupling for each resonant mode.

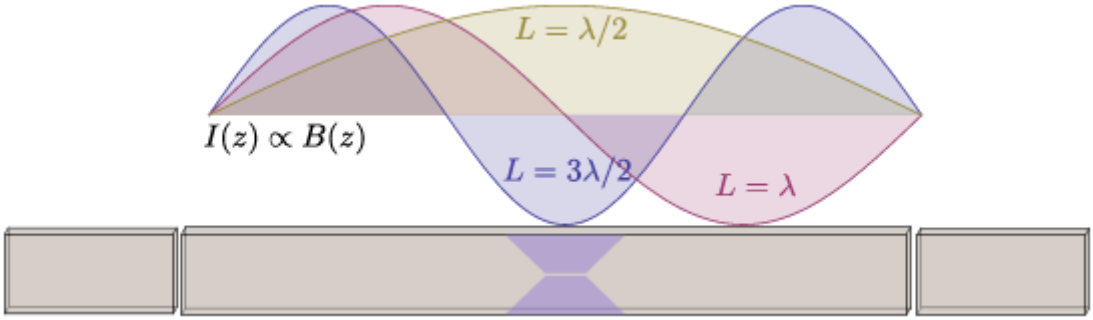

Figure 13: Magnetic distribution modes through the cavity. Although the first and third harmonic modes present a maximum field intensity where the constriction is made and the sample placed, the second harmonic does present a node, being the coupling between the sample and the circuit non-existing in this scenario. Reprinted from [20].

Parameters	Resonant mode 1	Resonant mode 3
N_{eff}	$2.39 \cdot 10^7$	$7.19 \cdot 10^7$
$g_{eff}/2\pi$	0.49 μHz	0.72 μHz

Table 2: Effective ensemble's size and coupling for each resonant mode. The circuits employed although being efficient lack of single spin coupling strength to provide an effective coupling non negligible.

As we can see, the values obtained for g_{eff} in both modes are absolutely negligible as compared to the photon dissipation and spin decoherence rates, and they are also well below the frequency resolution of the experiments. We recall that observing the phenomenom described in the previous section would require a collective coupling, $g\sqrt{N}$, comparable to the resonant frequency, ω_q, to not end with a tiny quotient in Eq.(25) as it is squared. According to our calculations (see Eq.(41) and Eq.(42)), this g_{eff} needs to be comparable to the dissipation terms γ and κ in order to have the double peak displayed in Fig.7. Although the double peak splitting can be enhanced by increasing the mean bosonic number $\langle b^\dagger b \rangle$ in addition to the effective coupling, this occupation does not suppose any difference; with the maximum driving we could introduce, i.e. the number of photons (about the same of spins in the sample to avoid distortion effects [20]) which in essence equals the electromagnetic wave intensity and this is proportional to the square of its amplitude, we cannot populate enough the sample due to the extremely weak coupling and so the weak interaction between the spins and the light.

Therefore, it seems that we cannot aim to observe the desired anti-crossing with these circuits. Besides the excellent quality of the parameters obtained with these kind of resonators, we need to explore which modifications in the resonator architecture could bring higher coupling intensities that could close the gap between the effective couplings obtained in Table 2 and the ones we need, approximately of the order of MHz, the same as γ [cf. Section 2]. Fortunately, we have the tools required to explore higher single spin couplings that could potentially give inspiring results.

3.3 Feasible potential improvements

Introducing nanoconstrictions in the resonators provided an enhancement in the reachable single spin couplings in that region due to the increase in the magnetic field intensity by forcing the same energy to flow in a narrower space. The data analyzed before were obtained for a 150 nm wide nanoconstriction (see Fig.9) but circuits with 30 nm wide and 10 μm long constrictions can be built, constituting the state of the art of this technology, and providing up to 50 kHz of intensity coupling for each S=1/2 spin. Taking into account these dimensions and that the DPPH has a density of $\rho = 1.4\ g/cm^3$ and a molecular weight of $M = 394.32 g/mol$ we end with $N \approx 1.92 \times 10^7\ spins$. We can estimate the new effective coupling with these new parameters. If we cool the system down to, let's say $T = 100\ mK$, to obtain the optimal effective number of spins, N_{eff}, in Eq.(44) and we work with a resonator of frequency $\omega_c \approx 3\ GHz$, so we tune the qubit transition frequency to be about $\omega_q \approx 1.5\ GHz$ to be in the resonant condition $\omega_c = 2\omega_q$, we end with an effective ensemble size of $N_{eff} \approx 1.18 \times 10^7$ and an effective coupling of $g_{eff} \approx 4\ Hz$. This results in an increment of 7 orders of magnitude respect to the values obtained in Table 2. Although it remains too small, it shows that increasing the single spin coupling, g, maintaining the spin density is crucial due to the cubic dependence in Eq.(25).

So far, we have been dealing with the lowest spin possible, S = 1/2, but working with single magnetic molecules which posses higher spins could be as well as improving the resonator's architecture a great option. Increasing the number of states that can interact with the magnetic field is reported to increase the single spin coupling, g, [17, 20] at least in a factor $\sqrt{S}$. Thus, working with the improved nanoconstrictions just presented combined with using samples of S > 1/2 could lead to a further enhancement in the effective coupling we seek. Examples of this kind of molecules could be the cluster $[Gd(H_2O)P_5W_{30}O_{110}]^{12-}$ [21], or GdW_{30}, whose ground state spin is 7/2 due to its Gd^{3+} ion trapped inside; the magnetic cluster compound $Mn_6O_4Br_4(Et_2dbm)_6$ [22] which contains 6 Mn^{3+} ions that add up to a total spin S = 12 in an octahedral simmetry; or, finally, the highest spin ground state reported [23], S = 91, of a giant $Ni_{20}Gd_{20}$ cage. In figure 14 we present the molecular structure of the first two single magnetic molecules.

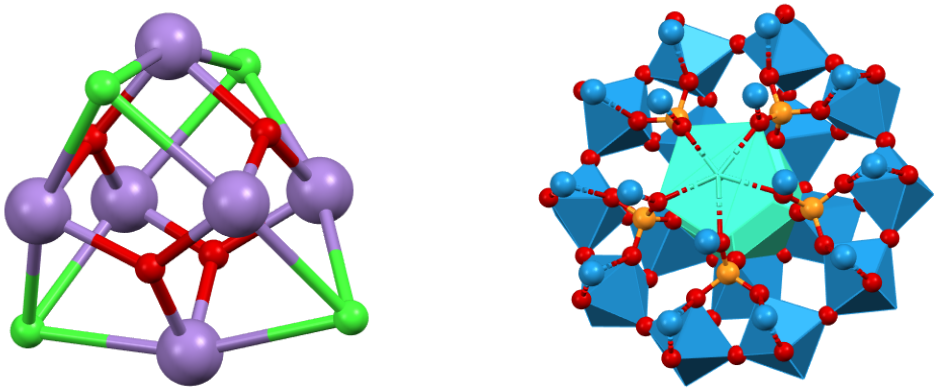

Figure 14: SMM that could suppose an improvement in the effective coupling measured to observe the one photon-two atoms anti-crossing. Left: Mn_6 octahedral core. Right: GdW_{30} cluster.

Conclusions & outlook

Now we proceed to summarize the main results obtained and the discussions made. After introducing our starting points in Section 1, in Section 2 studied the characteristics, both stationary and dynamic, of the system which can produce the entanglement between states with odd differing number of excitations. Finally, in Section 3, we explored the experimental possibilities that are available and determined the reachable values of the parameters, discussing the feasibility of observing the desired anticrossing.

Regarding the theoretical description, we observed how the anisotropy added to the Dicke model indeed allows transitions between states which differ in an odd number of excitations, more specifically, the creation of two excited states in the spin ensemble by one single photon, and vice versa. This occurs at a resonant magnetic field half as strong as the linear response; i.e. the Rabi oscillations which entangle one photon with one spin excitation. In addition, we obtain that a great coupling strength could displace this resonant condition for which we apply the harmonic approximation in the effective treatment of the dynamics. We demonstrate that the splitting amplitude of the anticrossing scales cubicly with the coupling intensity, confirming that the process we are dealing with is of third order. This splitting is reflected in the transmission spectrum as a double peak as we expected and shows a dependence not only with the effective coupling obtained from the effective treatment done in the resonant condition but also with the mean spin occupation; i.e. the number of spins excited in the sample. This shows that the system presents "feedback" as stronger the coupling of the ensemble to the cavity, the higher the number of qubits in its excited states, which leads to a greater splitting than if it only depended on the coupling strength. Finally we state the conditions required for the parameters to fulfill in order to be detected in a transmission experiment.

Moreover, we have explored the experimental setup required to observe this phenomenon. Based on experimental data, we have determined the best possible values for the parameters considered in our model compatible with state-ort-art coplanar waveguide resonators. Reaching an effective coupling for the two-spin transition stronger than the decoherence rate remains a very demanding condition as it requires taking the single-photon to single spin coupling to values that are beyond current technology. However, we pave the way for closing the gap by proposing feasible improvements both in the resonator's design and in the sample's nature. One of the best options to carry on in pursuing the observation of this effect is the study of samples with spin greater than $1/2$. Actually, the anisotropy needed in the system to exhibit the desired interaction usually occurs in samples with $S>1/2$. Our work shows that combining the improvements discussed in the resonator's architecture with this type of samples, we may not be so far from the conditions predicted to observe the coherent interaction between one photon and two collective spin states.

References

1. Garziano, L. *et al.* One photon can simultaneously excite two or more atoms. *Physical review letters* **117,** 043601 (2016).
2. Macrı, V., Nori, F., Savasta, S. & Zueco, D. Optimal spin squeezing in cavity QED based systems. *arXiv preprint arXiv:1902.10377* (2019).
3. Tóth, G. & Apellaniz, I. Quantum metrology from a quantum information science perspective. *Journal of Physics A: Mathematical and Theoretical* **47,** 424006 (2014).
4. Sakurai, J. J. *Advanced quantum mechanics* (Pearson Education India, 1967).
5. Cohen-Tannoudji, C., Dupont-Roc, J. & Grynberg, G. Photons and Atoms-Introduction to Quantum Electrodynamics. *Photons and Atoms-Introduction to Quantum Electrodynamics, by Claude Cohen-Tannoudji, Jacques Dupont-Roc, Gilbert Grynberg, pp. 486. ISBN 0-471-18433-0. Wiley-VCH, February 1997.,* 486 (1997).
6. Xie, Q., Zhong, H., Batchelor, M. T. & Lee, C. The quantum Rabi model: solution and dynamics. *Journal of Physics A: Mathematical and Theoretical* **50,** 113001 (2017).
7. Paz, J. P. & Zurek, W. H. in *Coherent atomic matter waves* 533–614 (Springer, 2001).
8. Breuer, H.-P., Petruccione, F., *et al. The theory of open quantum systems* (Oxford University Press on Demand, 2002).
9. Jaynes, E. T. & Cummings, F. W. Comparison of quantum and semiclassical radiation theories with application to the beam maser. *Proceedings of the IEEE* **51,** 89–109 (1963).
10. Kirton, P., Roses, M. M., Keeling, J. & Dalla Torre, E. G. Introduction to the Dicke model: From equilibrium to nonequilibrium, and vice versa. *Advanced Quantum Technologies* **2,** 1800043 (2019).
11. Dicke, R. H. Coherence in spontaneous radiation processes. *Physical review* **93,** 99 (1954).
12. Niemczyk, T. *et al.* Circuit quantum electrodynamics in the ultrastrong-coupling regime. *Nature Physics* **6,** 772–776 (2010).
13. Zhu, Y. *et al.* Vacuum Rabi splitting as a feature of linear-dispersion theory: Analysis and experimental observations. *Physical Review Letters* **64,** 2499 (1990).
14. Holstein, T. & Primakoff, H. Field dependence of the intrinsic domain magnetization of a ferromagnet. *Physical Review* **58,** 1098 (1940).
15. Hümmer, T., Reuther, G. M., Hänggi, P. & Zueco, D. Nonequilibrium phases in hybrid arrays with flux qubits and nitrogen-vacancy centers. *Physical Review A* **85,** 052320 (2012).
16. Rivas, A. & Huelga, S. F. *Open quantum systems* (Springer, 2012).
17. Jenkins, M. *et al.* Coupling single-molecule magnets to quantum circuits. *New Journal of Physics* **15,** 095007 (2013).
18. Jenkins, M. D. *et al.* Nanoscale constrictions in superconducting coplanar waveguide resonators. *Applied Physics Letters* **105,** 162601 (2014).
19. Jenkins, M. *et al.* A scalable architecture for quantum computation with molecular nanomagnets. *Dalton Transactions* **45,** 16682–16693 (2016).

20. Jenkins Sánchez, M. D. & Luis Vitalla, F. M. *Coupling Quantum Circuits to Magnetic Molecular Qubits* PhD thesis (Universidad de Zaragoza, Prensas de la Universidad).

21. Jenkins, M. *et al.* Coherent manipulation of three-qubit states in a molecular single-ion magnet. *Physical Review B* **95,** 064423 (2017).

22. Morello, A. *et al.* Long-range ferromagnetic dipolar ordering of high-spin molecular clusters. *Physical review letters* **90,** 017206 (2003).

23. Chen, W.-P. *et al.* Quantum Monte Carlo simulations of a giant {Ni 21 Gd 20} cage with a S= 91 spin ground state. *Nature communications* **9,** 1–6 (2018).

A Qubit Hamiltonian diagonalization

Dealing with N qubits with an energetic gap Δ between its levels and a bias term ϵ leads to the following qubit term Hamiltonian

$$H_q = \sum_{i=1}^{N} \left(\frac{\Delta}{2} \sigma_z^i + \frac{\epsilon}{2} \sigma_x^i \right) \equiv \sum_{i=1}^{N} H_q^i \tag{46}$$

We express the sum in terms of each individual Hamiltonian because it will be the same 2x2 matrix for every qubit (recall that we are supposing the same gap Δ and the same bias ϵ for every qubit):

$$H_q^i = \frac{1}{2} \begin{pmatrix} \Delta & \epsilon \\ \epsilon & -\Delta \end{pmatrix} \tag{47}$$

This gives us the following eigenvalues, W,

$$W_\pm \equiv \pm\sqrt{\Delta^2 + \epsilon^2}; \quad \omega_q \equiv \sqrt{\Delta^2 + \epsilon^2} \tag{48}$$

If we now define the relations

$$\sin\theta \equiv \frac{\epsilon}{\omega_q}; \quad \cos\theta \equiv \frac{\Delta}{\omega_q} \tag{49}$$

we obtain the following eigenvectors for the eigenvalues W_+ and W_-, respectively

$$|W_+\rangle \equiv \left(\cos\frac{\theta}{2}, \sin\frac{\theta}{2} \right); \quad |W_-\rangle \equiv \left(-\sin\frac{\theta}{2}, \cos\frac{\theta}{2} \right) \tag{50}$$

With these relations we can build the change of basis matrix, U, that will allow us to transform the operators, namely the Pauli matrices that define the Hamiltonian:

$$U = \begin{pmatrix} \cos\frac{\theta}{2} & -\sin\frac{\theta}{2} \\ \sin\frac{\theta}{2} & \cos\frac{\theta}{2} \end{pmatrix} \tag{51}$$

The transformation rule for changing the operator's basis, $A \to A'$, is given by:

$$A' = U^\dagger A U \tag{52}$$

which gives us for σ_x and σ_z:

$$\sigma_z^{i'} = \frac{1}{2} \begin{pmatrix} \omega_q & 0 \\ 0 & -\omega_q \end{pmatrix} \tag{53}$$

$$\begin{aligned} \sigma_x^{i'} &= \begin{pmatrix} \cos\frac{\theta}{2} & \sin\frac{\theta}{2} \\ -\sin\frac{\theta}{2} & \cos\frac{\theta}{2} \end{pmatrix} \begin{pmatrix} 0 & 1 \\ 1 & 0 \end{pmatrix} \begin{pmatrix} \cos\frac{\theta}{2} & -\sin\frac{\theta}{2} \\ \sin\frac{\theta}{2} & \cos\frac{\theta}{2} \end{pmatrix} = \\ &= \begin{pmatrix} 2\sin\frac{\theta}{2}\cos\frac{\theta}{2} & \cos^2\frac{\theta}{2} - \sin^2\frac{\theta}{2} \\ \cos^2\frac{\theta}{2} - \sin^2\frac{\theta}{2} & -2\sin\frac{\theta}{2}\cos\frac{\theta}{2} \end{pmatrix} = \cos\theta\sigma_x^i + \sin\theta\sigma_z^i \end{aligned} \tag{54}$$

These are the expressions that are used in the main text.

B Dynamics calculations

B.1 Equation of motion for mean values

Let the following expression be out quantum master equation which describes our open quantum system:

$$\dot{\rho} = -i[H, \rho] + \gamma \left(L\rho L^\dagger - \frac{1}{2}\{L^\dagger L, \rho\} \right) \tag{55}$$

where H is the system's Hamiltonian, γ some parameter which accounts for some dissipative effect and L the operator which describes that effect. If we now want to compute the temporal evolution of some operator mean value, $\langle \Theta \rangle$, we know that

$$\langle \Theta \rangle = Tr(\Theta\rho) \tag{56}$$

thus, supposing that the operator Θ does not depend explicitly on the time, $\dot{\Theta} = 0$,

$$\frac{d}{dt}\langle \Theta \rangle = Tr(\dot{\rho}\Theta = -iTr([H, \rho]\Theta) + \gamma \left(Tr(L\rho L^\dagger \Theta) - \frac{1}{2}Tr(L^\dagger L\rho\Theta) - \frac{1}{2}Tr(\rho L^\dagger L\Theta) \right) \tag{57}$$

But, applying the cyclical property of the trace:

$$Tr(ABC) = Tr(CAB) = Tr(BCA) \tag{58}$$

we can place in each term ρ in the right extreme:

$$\frac{d}{dt}\langle \Theta \rangle = -iTr(\Theta H\rho) + iTr(H\Theta\rho) + \gamma \left(Tr(L^\dagger \Theta L\rho) - \frac{1}{2}Tr(\{L^\dagger L, \Theta\}\rho) \right) \tag{59}$$

Finally, if we define

$$\mathcal{D}^\dagger_\Theta[L] \equiv L^\dagger \Theta L - \frac{1}{2}\{L^\dagger L, \Theta\} \tag{60}$$

it is easy to check that we end with

$$\frac{d}{dt}\langle \Theta \rangle = +i\langle [H, \Theta] \rangle + \gamma \left\langle \mathcal{D}^\dagger_\Theta[L] \right\rangle \tag{61}$$

This derivation is of course extensible to more dissipative parameters as we will work with now. It only introduces more terms like the second one in the last expression. In addition. it is worth to mention that if Θ commutes with L and $L^\dagger$, $\mathcal{D}^\dagger_\Theta[L] = 0$. This could happen if Θ and L act on different spaces or subsystems. In that case, the dissipator operator $\mathcal{D}$ cannot be non-zero due to the fact that the dissipation effect occurs inside one subsystem; i.e. neither the leakage of photons in the cavity due to its dissipation losses can affect to the spin coherence in the sample nor vice versa.

B.2 Dynamics for $\langle a \rangle$, $\langle b^2 \rangle$ and $\langle b^\dagger b \rangle$

Now that we have obtained how varies the mean value of an operator with the time under a certain dynamic given by the Hamiltonian and its master equation, we now proceed to compute these mean values for the operators of our interest. We recall here that we were working with

$$H_T = \omega_c a^\dagger a + \omega_q b^\dagger b + g_{eff}(ab^{\dagger 2} + a^\dagger b^2) + \alpha\kappa(e^{i\omega t} + e^{-i\omega t})(a + a^\dagger) \tag{62}$$

and

$$\dot{\rho} = -i[H_T, \rho] + \kappa \left(a\rho a^\dagger - \frac{1}{2}\{a^\dagger a, \rho\} \right) + \gamma \left(b\rho b^\dagger - \frac{1}{2}\{b^\dagger b, \rho\} \right) \tag{63}$$

A relation that we will be using throughout this calculations is the bosonic relation which applies both to a and b (and their h.c.):

$$[\xi, \xi^\dagger] = \xi\xi^\dagger - \xi^\dagger\xi = 1; \quad \xi = a, b \tag{64}$$

Hence, we start computing the evolution of $\langle a \rangle$:

$$\frac{d}{dt}\langle a \rangle = i \langle [H_T, a] \rangle + \kappa \left\langle \mathcal{D}_a^\dagger[a] \right\rangle \tag{65}$$

$$\begin{aligned} \langle [H_T, a] \rangle &= \omega_c \left\langle [a^\dagger a, a] \right\rangle + g_{eff} \left\langle b^2 [a^\dagger, a] \right\rangle + \alpha\kappa(e^{i\omega t} + e^{-i\omega t}) \left\langle [a^\dagger, a] \right\rangle = \\ &= -\omega_c \langle a \rangle - g_{eff} \langle b^2 \rangle - \alpha\kappa(e^{i\omega t} + e^{-i\omega t}) \end{aligned} \tag{66}$$

$$\begin{aligned} \left\langle \mathcal{D}_a^\dagger[a] \right\rangle &= \left\langle a^\dagger a a \right\rangle - \frac{1}{2}\left(\left\langle a^\dagger a a \right\rangle + \left\langle a a^\dagger a \right\rangle \right) = \frac{1}{2}\left(\left\langle a^\dagger a a \right\rangle - \left\langle a a^\dagger a \right\rangle \right) = \\ &= \frac{1}{2}\left(\left\langle (a a^\dagger - 1) a \right\rangle - \left\langle a a^\dagger a \right\rangle \right) = -\frac{1}{2}\langle a \rangle \end{aligned} \tag{67}$$

Merging these results we obtain

$$\frac{d}{dt}\langle a \rangle = -\left(i\omega_c + \frac{\kappa}{2} \right) \langle a \rangle - i g_{eff} \langle b^2 \rangle - i\alpha\kappa(e^{i\omega t} + e^{-i\omega t}) \tag{68}$$

Now, for $\langle b^2 \rangle$:

$$\frac{d}{dt}\langle b^2 \rangle = i \left\langle [\hat{H}_T, b^2] \right\rangle + \gamma \left\langle \mathcal{D}_{b^2}^\dagger[b] \right\rangle \tag{69}$$

$$\left\langle [\hat{H}_T, b^2] \right\rangle = \omega_q \left\langle [b^\dagger b, b^2] \right\rangle + g_{eff} \left\langle [a b^{\dagger 2}, b^2] \right\rangle \tag{70}$$

Let's calculate each commutator separately:

$$\begin{aligned} \left\langle [b^\dagger b, b^2] \right\rangle &= \left\langle b^\dagger b b b - b b b^\dagger b \right\rangle = \left\langle b^\dagger b b b - b \left(1 + b^\dagger b \right) b \right\rangle = \\ &= \left\langle [b^\dagger, b] b^2 - b^2 \right\rangle = -2 \langle b^2 \rangle \end{aligned} \tag{71}$$

$$\begin{aligned} \left\langle [a b^{\dagger 2}, b^2] \right\rangle &= \left\langle a [b^{\dagger 2}, b^2] \right\rangle = \left\langle a \left(b^\dagger b^\dagger b b - b b b^\dagger b^\dagger \right) \right\rangle = \\ &= \left\langle a \left(b^\dagger \left(b b^\dagger - 1 \right) b - b \left(1 + b^\dagger b \right) b^\dagger \right) \right\rangle = \left\langle a \left(b^\dagger b b^\dagger b - b^\dagger b - b b^\dagger - b b^\dagger b b^\dagger \right) \right\rangle = \\ &= \left\langle a \left(\left(b b^\dagger - 1 \right) b^\dagger b - b^\dagger b - \left(1 + b^\dagger b \right) - b b^\dagger b b^\dagger \right) \right\rangle = \left\langle a \left(b b^\dagger [b^\dagger, b] - 1 - 3 b^\dagger b \right) \right\rangle = \\ &= \left\langle a \left(\left(1 + b^\dagger b \right) (-1) - 1 - 3 b^\dagger b \right) \right\rangle = -2 \left\langle a \left(2 b^\dagger b + 1 \right) \right\rangle \end{aligned} \tag{72}$$

$$\begin{aligned} \left\langle \mathcal{D}_{b^2}^\dagger[b] \right\rangle &= \left\langle b^\dagger b^2 b \right\rangle - \frac{1}{2}\left\langle b^\dagger b b^2 \right\rangle - \frac{1}{2}\left\langle b^2 b^\dagger b \right\rangle = \frac{1}{2}\left(\left\langle b^\dagger b b b \right\rangle - \left\langle b b b^\dagger b \right\rangle \right) = \\ &= \frac{1}{2}\left(\left\langle b^\dagger b b b \right\rangle - \left\langle b \left(1 + b^\dagger b \right) b \right\rangle \right) = \frac{1}{2}\left(\left\langle [b^\dagger, b] b^2 \right\rangle - \langle b^2 \rangle \right) = -\langle b^2 \rangle \end{aligned} \tag{73}$$

Where all together reads:

$$\frac{d}{dt}\langle b^2 \rangle = -(i2\omega_q + \gamma) \langle b^2 \rangle - i2 g_{eff} \left\langle a(2 b^\dagger b + 1) \right\rangle \tag{74}$$

Finally, for $\langle b^\dagger b\rangle$:

$$\frac{d}{dt}\left\langle b^\dagger b\right\rangle = i\left\langle [H_T, b^\dagger b]\right\rangle + \gamma\left\langle \mathcal{D}^\dagger_{b^\dagger b}[b]\right\rangle \tag{75}$$

$$\left\langle [H_T, b^\dagger b]\right\rangle = g_{eff}\left\langle [ab^{\dagger 2} + a^\dagger b^2, b^\dagger b]\right\rangle = g_{eff}\left(\left\langle a[b^{\dagger 2}, b^\dagger b]\right\rangle + \left\langle a^\dagger [b^2, b^\dagger b]\right\rangle\right) \tag{76}$$

Like before, we compute each commutator separately:

$$\begin{aligned}[b^{\dagger 2}, b^\dagger b] &= (b^\dagger b^\dagger b^\dagger b - b^\dagger b b^\dagger b^\dagger) = b^\dagger b^\dagger b^\dagger b - b^\dagger(1 + b^\dagger b)b^\dagger = \\ &= b^{\dagger 2}[b^\dagger, b] - b^{\dagger 2} = -2b^{\dagger 2}\end{aligned} \tag{77}$$

$$\begin{aligned}[b^2, b^\dagger b] &= (bbb^\dagger b - b^\dagger bbb) = b(1 + b^\dagger b)b - b^\dagger bbb = \\ &= [b, b^\dagger]b^2 + b^2 = 2b^2\end{aligned} \tag{78}$$

$$\begin{aligned}\left\langle \mathcal{D}^\dagger_{b^\dagger b}[b]\right\rangle &= \left\langle b^\dagger b^\dagger bb\right\rangle - \frac{1}{2}\left\langle b^\dagger bb^\dagger b\right\rangle - \frac{1}{2}\left\langle b^\dagger bb^\dagger b\right\rangle = \\ &= \left\langle b^\dagger b^\dagger bb\right\rangle - \left\langle b^\dagger bb^\dagger b\right\rangle = \left\langle b^\dagger [b^\dagger, b]b\right\rangle = -\left\langle b^\dagger b\right\rangle\end{aligned} \tag{79}$$

Thus,

$$\frac{d}{dt}\left\langle b^\dagger b\right\rangle = i2g_{eff}\left(\left\langle a^\dagger b^2\right\rangle - \left\langle ab^{\dagger 2}\right\rangle\right) - \gamma\left\langle b^\dagger b\right\rangle \tag{80}$$

With this we obtain the equation system that appears in the main text:

$$\begin{cases} \dfrac{d}{dt}\langle a\rangle = -\left(i\omega_c + \dfrac{\kappa}{2}\right)\langle a\rangle - ig_{eff}\left\langle b^2\right\rangle - i\alpha\kappa\left(e^{i\omega t} + e^{-i\omega t}\right) & \text{(81a)} \\ \dfrac{d}{dt}\left\langle b^2\right\rangle = -(i2\omega_q + \gamma)\left\langle b^2\right\rangle - i2g_{eff}\left\langle a\left(2b^\dagger b + 1\right)\right\rangle & \text{(81b)} \\ \dfrac{d}{dt}\left\langle b^\dagger b\right\rangle = i2g_{eff}\left(\left\langle a^\dagger b^2\right\rangle - \left\langle ab^{\dagger 2}\right\rangle\right) - \gamma\left\langle b^\dagger b\right\rangle & \text{(81c)} \end{cases}$$

B.3 RWA and MF approximations

Now, in order to be able to solve these equations analytically, we resort to a couple of approximations: mean field theory, which allows us to consider that the mean values of each operator is independient from each other, so

$$\langle AB\rangle = \langle A\rangle\langle B\rangle \tag{82}$$

and the rotating wave approximation. In the latter, we place ourselves in the interaction picture and suppose that the the cavity operators rotate with the same frequency as the driving, ω, and the spins with ω'. If we place ourselves in this rotating frame:

$$\begin{cases} \langle a\rangle = \langle\tilde{a}\rangle e^{-i\omega t} & \text{(83a)} \\ \langle b\rangle = \left\langle\tilde{b}\right\rangle e^{-i\omega' t} & \text{(83b)} \end{cases}$$

and we proceed to apply these approximations to the system.

Starting with $\langle a\rangle$:

$$\frac{d}{dt}\langle a\rangle = \frac{d}{dt}\langle\tilde{a}\rangle e^{-i\omega t} - i\omega\langle\tilde{a}\rangle e^{-i\omega t} = -\left(i\omega_c + \frac{\kappa}{2}\right)\langle\tilde{a}\rangle e^{-i\omega t} - ig_{eff}\left\langle\tilde{b}^2\right\rangle - i\alpha\kappa(e^{i\omega t} + e^{-i\omega t}) \tag{84}$$

If we now extract $e^{-i\omega t}$ as common factor and we apply that $\omega = 2\omega'$, which is the resonant condition that interests us:

$$\frac{d}{dt}\langle\tilde{a}\rangle = -\left(i(\omega_c-\omega)+\frac{\kappa}{2}\right)\langle\tilde{a}\rangle - ig_{eff}\left\langle\tilde{b}^2\right\rangle - i\alpha\kappa(e^{i2\omega t}+1) \tag{85}$$

For $\langle b^2\rangle$:

$$\frac{d}{dt}\langle b^2\rangle = \frac{d}{dt}\left\langle\tilde{b}^2\right\rangle e^{i2\omega' t} - i2\omega'\left\langle\tilde{b}^2\right\rangle e^{-i2\omega' t} \tag{86}$$

$$\frac{d}{dt}\langle b^2\rangle = -\left(i2\omega_q+\gamma\right)\left\langle\tilde{b}^2\right\rangle e^{-i2\omega' t} - i2g_{eff}\langle\tilde{a}\rangle e^{-i\omega t}\left(2\left\langle b^{\tilde{\dagger}}b\right\rangle+1\right) \tag{87}$$

And, again, applying that $\omega = 2\omega'$:

$$\frac{d}{dt}\left\langle\tilde{b}^2\right\rangle = -\left(i\left(2\omega_q-\omega\right)+\gamma\right)\left\langle\tilde{b}^2\right\rangle - i2g_{eff}\langle\tilde{a}\rangle\left(2\left\langle b^{\tilde{\dagger}}b\right\rangle+1\right) \tag{88}$$

Finally, for $\left\langle b^{\tilde{\dagger}}b\right\rangle$, applying MF:

$$\frac{d}{dt}\left\langle b^{\dagger}b\right\rangle = \frac{d}{dt}\left\langle b^{\tilde{\dagger}}b\right\rangle = -\gamma\left\langle b^{\tilde{\dagger}}b\right\rangle - i2g_{eff}\left(\langle\tilde{a}\rangle e^{-i\omega t}\left\langle\tilde{b}^{\dagger 2}\right\rangle e^{i2\omega t} - h.c.\right) \tag{89}$$

$$\frac{d}{dt}\left\langle b^{\tilde{\dagger}}b\right\rangle = -\gamma\left\langle b^{\tilde{\dagger}}b\right\rangle - i2g_{eff}\left(\langle\tilde{a}\rangle\left\langle\tilde{b}^{\dagger 2}\right\rangle - h.c.\right) \tag{90}$$

Which gives us the following system of equations in this frame:

$$\begin{cases} \frac{d}{dt}\langle\tilde{a}\rangle = -\left(i\left(\omega_c-\omega\right)+\frac{\kappa}{2}\right)\langle\tilde{a}\rangle - ig_{eff}\left\langle\tilde{b}^2\right\rangle - i\alpha\kappa\left(e^{i2\omega t}+1\right) & \text{(91a)} \\ \frac{d}{dt}\left\langle\tilde{b}^2\right\rangle = -\left(i\left(2\omega_q-\omega\right)+\gamma\right)\left\langle\tilde{b}^2\right\rangle - i2g_{eff}\langle\tilde{a}\rangle\left(2\left\langle b^{\tilde{\dagger}}b\right\rangle+1\right) & \text{(91b)} \\ \frac{d}{dt}\left\langle b^{\tilde{\dagger}}b\right\rangle = -\gamma\left\langle b^{\tilde{\dagger}}b\right\rangle - i2g_{eff}\left(\langle\tilde{a}\rangle\left\langle\tilde{b}^{\dagger 2}\right\rangle - h.c.\right) & \text{(91c)} \end{cases}$$

Finally, in order to obtain the stationary solutions that will be used for the transmission calculation, we neglect oscillating terms and suppose the stationary state $t \to 0$ and $d/dt \to 0$

$$\begin{cases} \langle\tilde{a}\rangle = -\frac{i2}{\kappa}\left[\alpha\kappa + g_{eff}\left\langle\tilde{b}^2\right\rangle + \left(\omega_c-\omega\right)\langle\tilde{a}\rangle\right] & \text{(92a)} \\ \left\langle\tilde{b}^2\right\rangle = -\frac{i2}{\gamma}\left[g_{eff}\langle\tilde{a}\rangle\left(2\left\langle b^{\tilde{\dagger}}b\right\rangle+1\right) + \frac{1}{2}\left(2\omega_q-\omega\right)\left\langle\tilde{b}^2\right\rangle\right] & \text{(92b)} \\ \left\langle b^{\tilde{\dagger}}b\right\rangle = -\frac{i2}{\gamma}\left(\langle\tilde{a}\rangle\left\langle\tilde{b}^{\dagger 2}\right\rangle - h.c.\right) & \text{(92c)} \end{cases}$$

B.4 Solutions with physical meaning

We proceed to solve this closed system and for that we simplify the notation defining

$$\mathcal{A} \equiv \frac{2\alpha\kappa}{\kappa}; \quad \mathcal{G}_\kappa \equiv \frac{2g_{eff}}{\kappa}; \quad \mathcal{G}_\gamma \equiv \frac{2g_{eff}}{\gamma} \tag{93}$$

$$X \equiv i\langle\tilde{a}\rangle; \quad Y \equiv \left\langle\tilde{b}^2\right\rangle; \quad Z \equiv \left\langle b^{\tilde{\dagger}}b\right\rangle \tag{94}$$

so the equations read:

$$\begin{cases} X = (\mathcal{A} + \mathcal{G}_\kappa Y) & \text{(95a)} \\ Y = -X\mathcal{G}_\gamma(2Z+1) & \text{(95b)} \\ Z = -\mathcal{G}_\gamma(XY^* + X^*Y) & \text{(95c)} \end{cases}$$

Introducing the expression for Y in Z and we do so also in X we obtain the following system of two equations for Z and X:

$$\begin{cases} X = \dfrac{\mathcal{A}}{1 + \mathcal{G}_\kappa \mathcal{G}_\gamma(2Z+1)} & \text{(96a)} \\ Z = \dfrac{2\mathcal{G}_\gamma^2 |X|^2}{1 - 4\mathcal{G}_\gamma^2 |X|^2} & \text{(96b)} \end{cases}$$

We know that Z has to be a real number since the mean bosonic occupation $\langle b^\dagger b \rangle$ has to be so. By looking directly the expression for X we note that it has to be real either which leads to the conclusion that $\langle a \rangle$ is purely imaginary due to how is defined X. In addition, if we solve this system we end with a third order equation for X, which gives three solutions. However, only one should be the "real", the one with physical meaning. If we continue examining each variable as before, we obtain that if $X \in \mathcal{R}$ then $Y \in \mathcal{R}$. Moreover, Z has to be positive (we cannot have a negative number of spins in their excited state) so X and Y must have contrary signs. Now only remains to assign which sign correspond to X and Y: if $Y > 0$, X would be also positive due to the fact that, without loss of generality, $\mathcal{A}$ and $\mathcal{G}_\kappa$ are both positive. So Y has to be negative and we obtain the last restriction for X:

$$Y = \frac{X - \mathcal{A}}{\mathcal{G}_\kappa} < 0 \implies X < \mathcal{A} \tag{97}$$

which makes sense if we think about it as that the annihilation operator cannot be greater than the ratio of photons we introduce through the driving and the photon losses by the dissipation in the cavity.

With all these considerations we can solve for X and we obtain:

$$\mathcal{F}(X) \equiv -4\mathcal{G}_\gamma X^3 + 4\mathcal{G}_\gamma^2 \mathcal{A} X^2 + (1 + \mathcal{G}_\gamma \mathcal{G}_\kappa) X - \mathcal{A} \tag{98}$$

for which as we can see in Fig.15 only has one solution that obeys all the restrictions imposed before.

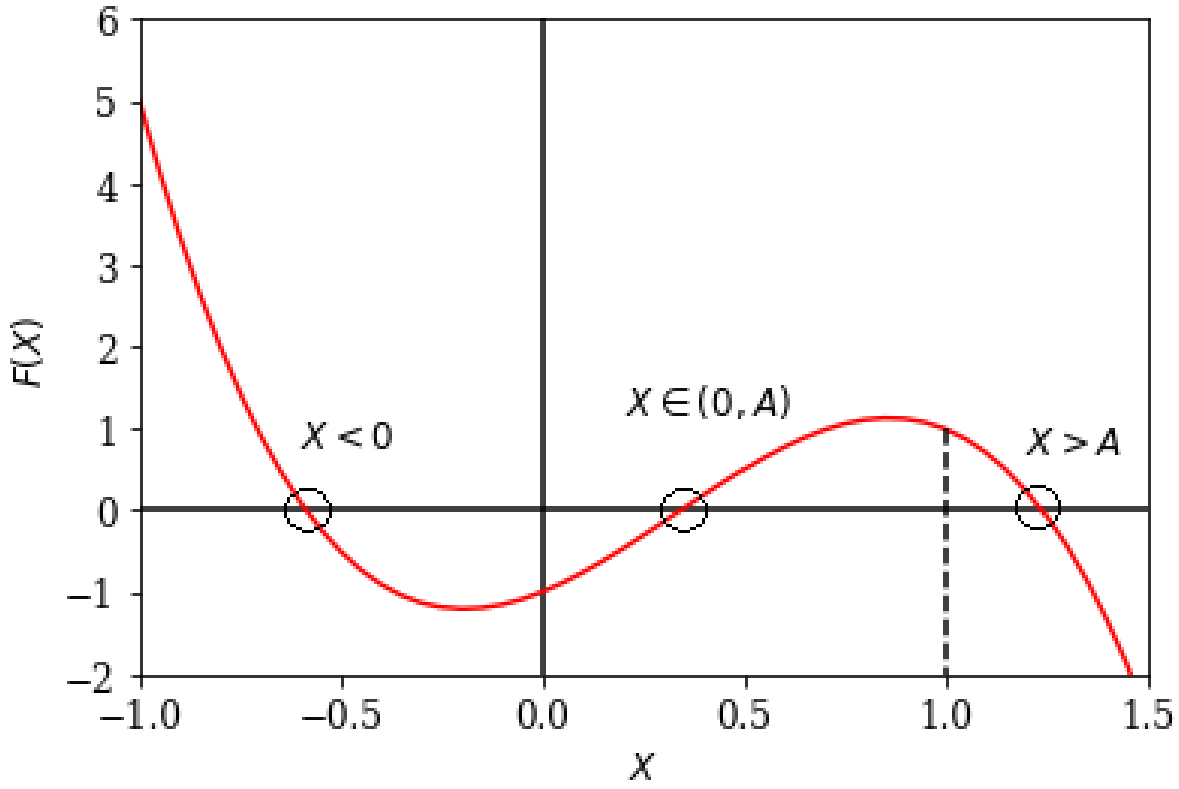

Figure 15: Graphical solution for Eq.(98) for $\mathcal{G}_\gamma = \mathcal{G}_\kappa = \mathcal{A} = 1$. The vertical dashed line indicates the value of $\mathcal{A}$.